AMERICAN SOCIETY FOR MICROBIOLOGY | Journal of Virology®

PATHOGENESIS AND IMMUNITY

A Novel Murine Model Expressing a Chimeric mSCARB2/hSCARB2 Receptor Is Highly Susceptible to Oral Infection with Clinical Isolates of Enterovirus 71

Cheng-Hung Yang,[a] Chung-Tiang Liang,[b] Si-Tse Jiang,[c,d] Kuan-Hsing Chen,[e] Chun-Chiao Yang,[a] Mei-Ling Cheng,[a,f,g,h] Hung-Yao Ho[a,f,g,i,j]

[a]Graduate Institute of Biomedical Science, Chang Gung University, Guishan, Taoyuan, Taiwan
[b]Novo Nordisk Research Centre, Department of Animal Facility, Discovery Biology, Beijing, China
[c]National Laboratory Animal Center, National Applied Research Laboratories, Taipei, Taiwan
[d]Institute of Clinical Medicine, College of Medicine, National Cheng Kung University, Tainan, Taiwan
[e]Kidney Research Center, Chang Gung Memorial Hospital at Linkou, Guishan, Taoyuan, Taiwan
[f]Healthy Aging Research Center, Chang Gung University, Guishan, Taoyuan, Taiwan
[g]Clinical Phenome Center, Chang Gung Memorial Hospital at Linkou, Guishan, Taoyuan, Taiwan
[h]Department of Biomedical Sciences, College of Medicine, Chang Gung University, Taoyuan, Taiwan
[i]Department of Medical Biotechnology and Laboratory Science, College of Medicine, Chang Gung University, Taoyuan, Taiwan
[j]Research Center for Emerging Viral Infections, Chang Gung University, Taoyuan, Taiwan

ABSTRACT Enterovirus 71 (EV71) infection is generally associated with hand-foot-and-mouth disease (HFMD) and may cause severe neurological disorders and even death. An effective murine oral infection model for studying the pathogenesis of various clinical EV71 isolates is lacking. We developed a transgenic (Tg) mouse that expresses an EV71 receptor, that is, human scavenger receptor class B member 2 (hSCARB2), in a pattern highly similar to that of endogenous murine SCARB2 (mSCARB2) protein. A FLAG-tagged *SCARB2* cDNA fragment composed of exons 3 to 12 was inserted into a murine *Scarb2* gene-containing bacterial artificial chromosome (BAC) clone, and the resulting transgene was used for establishment of chimeric receptor-expressing Tg mice. Tg mice intragastrically (i.g.) infected with clinical isolates of EV71 showed neurological symptoms, such as ataxia and paralysis, and fatality. There was an age-dependent decrease in susceptibility to viral infection. Pathological characteristics of the infected Tg mice resembled those of encephalomyelitis in human patients. Viral infection was accompanied by microglial activation. Clodronate treatment of the brain slices from Tg mice enhanced viral replication, while lipopolysaccharide treatment significantly inhibited it, suggesting an antiviral role for microglia during EV71 infection. Taken together, this Tg mouse provides a model that closely mimics natural infection for studying EV71 pathogenesis and for evaluating the efficacy of vaccines or other antiviral drugs.

IMPORTANCE The availability of a murine model of EV71 infection is beneficial for the understanding of pathogenic mechanisms and the development and assessment of vaccines and antiviral drugs. However, the lack of a murine oral infection model thwarted the study of pathogenesis induced by clinically relevant EV71 strains that are transmitted via the oral-oral or oral-fecal route. Our Tg mice could be intragastrically infected with clinically relevant EV71 strains in an efficient way and developed neurological symptoms and pathological changes strikingly resembling those of human infection. Moreover, these mice showed an age-dependent change in susceptibility that is similar to the human case. This Tg mouse, when combined with the use of other genetically modified mice, potentially contributes to studying the relationship between developmental changes in immunity and susceptibility to virus.

Citation Yang C-H, Liang C-T, Jiang S-T, Chen K-H, Yang C-C, Cheng M-L, Ho H-Y. 2019. A novel murine model expressing a chimeric mSCARB2/hSCARB2 receptor is highly susceptible to oral infection with clinical isolates of enterovirus 71. J Virol 93:e00183-19. https://doi.org/10.1128/JVI.00183-19.

Editor Susana López, Instituto de Biotecnologia/UNAM

Address correspondence to Hung-Yao Ho, hoh01@mail.cgu.edu.tw.

Received 6 February 2019
Accepted 15 March 2019
Accepted manuscript posted online 20 March 2019
Published 15 May 2019

KEYWORDS SCARB2, enterovirus 71, oral infection

Enterovirus 71 (EV71), a single-positive-strand RNA virus, is taxonomically classified as human enterovirus species A of the genus *Enterovirus* of the family *Picornaviridae*. It consists of a core of positive-sense single-stranded RNA surrounded by an icosahedral capsid. The capsid is composed of 60 protomers, each of which is made up of four structural proteins, namely, VP1, VP2, VP3, and VP4. EV71 and another enterovirus, coxsackievirus A16 (CVA16), are common etiological agents of hand-foot-and-mouth disease (HFMD) and are transmitted predominantly from feces, saliva, or respiratory droplets of infected individuals to others via the fecal-oral or oral-oral route (1). The disease is generally self-limiting and is characterized by a mild fever with ulcers in the oral cavity, a papulovesicular rash on extremities, and herpangina. A few patients develop severe neurological manifestations, such as encephalitis, aseptic meningitis, and acute flaccid paralysis, and cardiopulmonary symptoms. HFMD became an endemic health problem in Asia-Pacific countries, including Taiwan, Malaysia, Singapore, Hong Kong, South Korea, and Japan (1, 2). The largest epidemic to date occurred in China. Nearly 489,000 cases and a mortality rate of 0.026% were reported in 2008 (3). A total of 3 million cases and about 1,500 deaths have been reported (4, 5).

A number of cellular receptors for EV71 have been identified. These include human scavenger receptor class B2 (hSCARB2) (6), P-selectin glycoprotein ligand 1 (PSGL1) (7), annexin II (8), and nucleolin (9). SCARB2 is a type III glycoprotein localized to the membrane of late endosomes and lysosomes and consists of a large domain projecting into the lumen and a short cytoplasmic domain. Being an abundant lysosomal protein, SCARB2 is involved in membrane trafficking and reorganization of the endosome and lysosome (10). Exogenous expression of hSCARB2 mediated infection of L929 cells with all EV71 strains tested (11), while murine SCARB2 (mSCARB2) was 40 to 100 times less efficient in doing so (12). The hSCARB2 protein and its mouse counterpart share over 85% identity and 99% similarity in amino acid sequence. A domain swapping study pinpointed that the amino acid stretch (amino acids 142 to 204) encoded by *SCARB2* exon 4 is critical for virion binding.

Proper animal models are required for studying the pathogenic mechanism of EV71 and for testing the efficacy of vaccines and antiviral pharmaceuticals. Nonhuman primates, such as rhesus, cynomolgus, and African green monkeys, developed neurological symptoms upon EV71 infection (13–17). Although these monkeys can adequately model the neurological complications of human infection, it is difficult to use them owing to ethical issues and the high cost of maintenance. Moreover, the lack of genetically modified monkeys hampered the study of the pathogenic mechanism through a genetic approach. The mouse became an attractive alternative for development of an EV71 infection model. Different strategies, such as neonatal mouse infection, inoculation with mouse-adapted virus, and the use of immunodeficient genetically modified mice, have been employed to develop infection models. Yu et al. successfully infected neonatal ICR mice at an age of up to 3 days with TW/4643/98 virus via the intraperitoneal (i.p.) route (18). It is relatively difficult to handle suckling mice. There appears to be an age-dependent change in viral susceptibility. Mice aged $>$14 days are normally resistant to experimental viral infection (19). The virus has been adapted in mice to facilitate its oral inoculation (19, 20). Wang et al. reported that 7-day-old ICR mice orally infected with mouse-adapted strain MP4 succumbed to poliomyelitis-like paralysis and death (19). Using another mouse-adapted strain, MAVS, Ong et al. showed that 1 out of 10 orally infected 2-week-old mice had paralytic symptoms (20). However, the mouse-adapted viruses are different in sequence composition from their parental strain (19) and, depending on the adaptation method, display tropism for particular mouse tissues (19, 21). These differences may distort our understanding of the pathogenic mechanism of clinically relevant strains. Other research groups have resorted to the use of immunodeficient mice for the establishment of mouse infection models. NOD/SCID mice that had been intracerebrally (i.c.), intraperitoneally, or intragastrically

(i.g.) infected developed skin rash and paralytic symptoms and were destined to die (22, 23). Additionally, AG129 mice lacking interferon alpha/beta (IFN-α/β) and interferon gamma receptors were susceptible to oral and i.p. EV71 infections up to the age of 2 weeks (24). *stat-1* knockout mice defective in interferon signaling developed paralysis after intraperitoneal virus inoculation (22). The use of immunodeficient mice obscures the roles of immunity in the pathogenesis of EV71 infection.

The discovery of EV71 receptors prompted researchers to derive receptor transgenic (Tg) mice for establishment of an infection model. A transgenic mouse that expresses hSCARB2 from the EF-1α promoter developed paralytic symptoms after subcutaneous injection of virus (25). Fujii et al. used a human *SCARB2* gene-containing bacterial artificial chromosome (BAC) to generate a transgenic mouse line (26). Three-week-old transgenic mice were susceptible to EV71 infection via the i.c., intravenous (i.v.), and i.p. routes. A high percentage of the infected mice had neurological symptoms and died. Only 1/20 transgenic mice could be successfully infected with the Isehara (genotype C) strain via the i.g. route. The low susceptibility of these mice to oral infection prompted us to develop a new oral EV71 infection model.

In the present study, we established a BAC Tg mouse strain that expresses a chimeric mSCARB2/hSCARB2 receptor. Tg mice at ages of up to 3 weeks are susceptible to intragastric infection with a clinically relevant EV71 strain. The infected mice develop neuropathology and symptoms, such as ataxia and limb paralysis, and even die. Microglial proliferation, as evident by increased immunohistochemical (IHC) staining for the microglial activation marker Iba1, serves as an antiviral immune response. Polarization of microglia toward an M1 phenotype promotes antiviral immunity. The present model simulates the natural route of EV71 infection and is useful for studying its pathogenesis and for pharmacological evaluation of antiviral drugs or vaccines.

RESULTS

Generation of a Tg mouse that expresses the mSCARB2/hSCARB2 chimeric receptor. To construct the recombinant BAC, we inserted a human *SCARB2* cDNA fragment in the mouse BAC in such a way that the genomic sequence of the *Scarb2* gene up to exon 3 was fused in-frame with the human cDNA sequence (Fig. 1A). This recombinant BAC is supposed to drive the expression of a FLAG-tagged chimeric receptor and was used for the generation of a BAC transgenic mouse. Four founder mice [C57BL/6J-Tg(*Scarb2-SCARB2*)] were obtained. Genomic DNA was isolated from these mice for genotyping. A PCR product of the expected size was amplified from the genomic DNA of Tg mice but not from that of non-Tg mice (Fig. 1A). Hemizygous C57BL/6J-Tg(*Scarb2-SCARB2*)3 mice, designated Tg3 mice, were used throughout the present study. Similar findings were obtained for the mice of another founder line, Tg1 mice.

Expression profile of the mSCARB2/hSCARB2 chimeric protein in Tg mouse. To examine the expression of the mSCARB2/hSCARB2 chimeric protein across different tissues, we prepared tissue homogenates and performed Western blotting with an anti-hSCARB2 antibody (Fig. 1B, top) or an anti-FLAG antibody (Fig. 1B, middle). The anti-hSCARB2 antibody used binds more specifically to human than mouse protein. The immunoblot with anti-hSCARB2 antibody showed that the chimeric protein was expressed in Tg mice. In a similar fashion, anti-FLAG antibody detected the chimeric protein, which was similar in size to the endogenous protein (i.e., that of non-Tg mice) cross-reactive with anti-hSCARB2 antibody. It was highly expressed in tissues such as liver, spleen, lung, stomach, duodenum, jejunum, ileum, and colon and was expressed to a lesser extent in heart, cerebrum, cerebellum, and spinal cord (Fig. 1). The expression pattern of the chimeric receptor is similar to that of the endogenous protein (Fig. 1B, bottom). The only exception is that the levels of the anti-FLAG antibody-detectable protein in the duodenum and jejunum were low, presumably owing to the presence of FLAG tag-cleaving enterokinase in these tissues. Consistent with the immunoblotting results, IHC analysis revealed that the mSCARB2/hSCARB2 chimeric protein was specifically expressed in Tg mice. The chimeric protein was expressed to a relatively high level

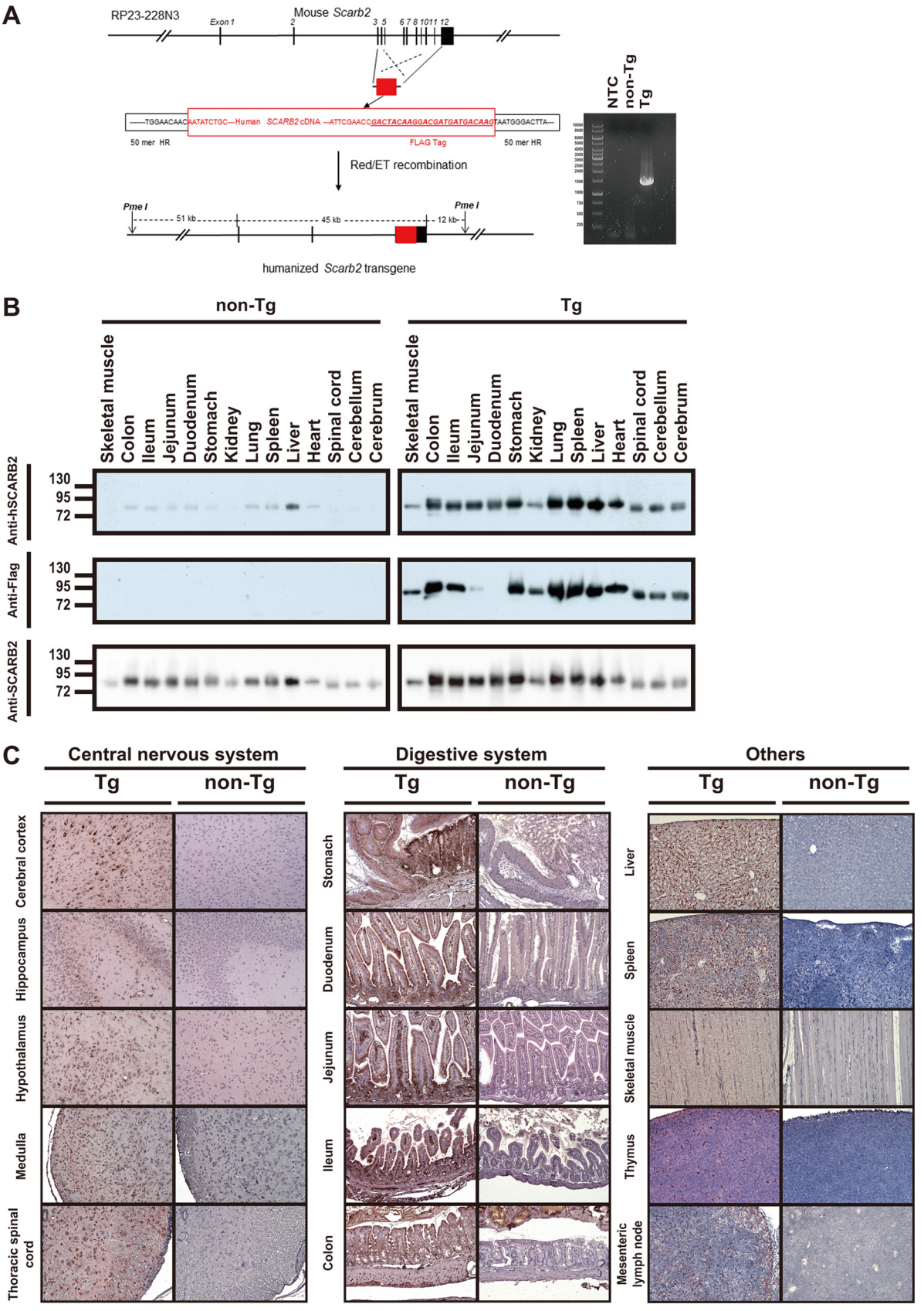

FIG 1 Expression of mSCARB2/hSCARB2 in *Scarb2-SCARB2* BAC Tg mice. (A) Schematic diagram showing the construction of the recombinant BAC. The RP23-228N3 clone is shown at the top. The genomic sequence spanning from exon 3 to exon 12 was replaced with the

(Continued on next page)

in different parts of the central nervous system (CNS). Apparently, neurons expressed more chimeric protein than did glial cells or endothelial cells. Additionally, the protein was expressed in various sections of the digestive tract. Epithelial cells and smooth muscle cells were distinctly stained in these sections. Moreover, the chimeric protein was found in muscle, liver, thymus, mesenteric lymph nodes, and spleen (Fig. 1C).

Increased susceptibility of Tg mice to EV71 infection via the intragastric route. To examine whether Tg mice are susceptible to EV71 infection, we inoculated the Tg mice and their non-Tg littermates with the clinically relevant viruses via different routes. The Tg mice, which were inoculated i.g. with EV71/TW/4643/98 (EV71-4643) at 10^8 PFU, showed ataxia, limb paralysis, and death (Fig. 2A and B; see also Movies S1 to S3 in the supplemental material). Non-Tg mice were resistant to EV71 infection, as no neurological symptom was observed in infected non-Tg mice (data not shown). Similar findings were obtained with other clinically relevant strains, EV71/TW/1743/98 (EV71-1743) and EV71 Fuyang (EV71-Fy) (Fig. 2I to K). It appeared that the clinical severity and survival of orally infected mice were dependent on the inoculum dose of the virus. A reduction in the inoculum dose led to abatement of clinical symptoms and to enhanced survival (Fig. 2C and D). Age can be an important determinant of susceptibility to virus. The susceptibility of Tg mice to oral infection decreased with their age, and Tg mice at the age of 28 days were refractory to infection (Fig. 2E to G). Tg mice were susceptible to infection via the i.p. and i.c. routes. Infection of Tg mice with the virus at 10^6 PFU via the i.p. route resulted in the development of neurological symptoms and death (Fig. 2M and N). An inoculum dose-dependent effect was also observed (Fig. 2M to P). Tg mice at the age of 1 year succumbed to infection via the i.c. route of inoculation (Fig. 2H and L). Consistent with the previous finding that CVA16 uses hSCARB2 for host cell entry (6), the Tg mice developed neurological symptoms and even died after intragastric infection with CVA16 at the ages of 14 and 21 days (Fig. 2Q to S).

EV71 replication in various tissues of Tg mice. To study the sites of EV71 replication in Tg mice, we inoculated 2-week-old Tg mice and non-Tg littermates via the i.g. route and employed IHC analysis to detect EV71 VP2 protein in their tissues. For the Tg mice that displayed neurological symptoms, VP2 protein was expressed in CNS tissues such as cerebral cortex, hippocampus, cerebellum, medulla, pons, and thoracic spinal cord (Fig. 3A). Additionally, VP2 was detected in skeletal muscle, albeit to a lesser extent, in the majority of hind-limb-paralyzed mice. However, the skeletal muscle of moribund mice was strongly positive for VP2. Interestingly, VP2 was detected in the paw of a few infected mice. No VP2 protein was expressed in tissues of non-Tg mice (data not shown), and the tissues were histologically normal (data not shown). Close examination of hematoxylin and eosin (H&E)-stained sections revealed focal neuronal necrosis and cell loss in hippocampal Ammon's horn (cornu ammonis [CA]), in particular CA2 and CA3. The neuronal loss became more severe in areas of the inferior colliculus. There was focal infiltration of microglia adjacent to degenerating or dying neurons, suggesting the occurrence of neuronophagia. Sections through the midbrain at the level of the inferior colliculus and through the pons showed more extensive neuronal loss in the pons than in hippocampal CA2 (Fig. 3A). Neuropil vacuolization in these areas was observed. Neuronal shrinkage, nuclear fragmentation, and the appearance of

FIG 1 Legend (Continued)
corresponding part of human *SCARB2* cDNA that carries a FLAG tag-coding sequence. The resulting clone carrying the humanized *Scarb2* transgene is displayed at the bottom. PCR genotyping of the Tg mice is also shown. Genomic DNAs isolated from Tg3 and non-Tg mice were subjected to PCR genotyping as described in Materials and Methods. The amplified product for the Tg sample is 1,511 bp long. NTC, no-template control. (B) Tissue distribution of the mSCARB2/hSCARB2 chimeric protein in Tg mice. (Top and middle) Tg and non-Tg mice were sacrificed, and cerebrum, cerebellum, spinal cord, heart, liver, spleen, lung, stomach, duodenum, jejunum, ileum, colon, kidney, and skeletal muscle were harvested for Western blotting with anti-hSCARB2 (top) and anti-FLAG (middle) antibodies. It should be noted that the anti-hSCARB2 antibody is known to cross-react with the murine endogenous protein. (Bottom) The immunoblot membrane shown in the top panel was stripped and reprobed with anti-SCARB2 antibody, which can react with both murine and human proteins. A representative result out of three experiments is shown. (C) IHC analysis of expression of the chimeric protein in Tg mice. Cerebral cortex, hippocampus, hypothalamus, medulla, thoracic spinal cord, stomach, duodenum, jejunum, ileum, colon, liver, spleen, skeletal muscle, thymus, and mesenteric lymph nodes were collected from the Tg mice; paraffinized; sectioned for immunohistochemical staining with the anti-hSCARB2 antibody; and counterstained with hematoxylin. Original magnification, ×200. A representative result out of three experiments is shown.

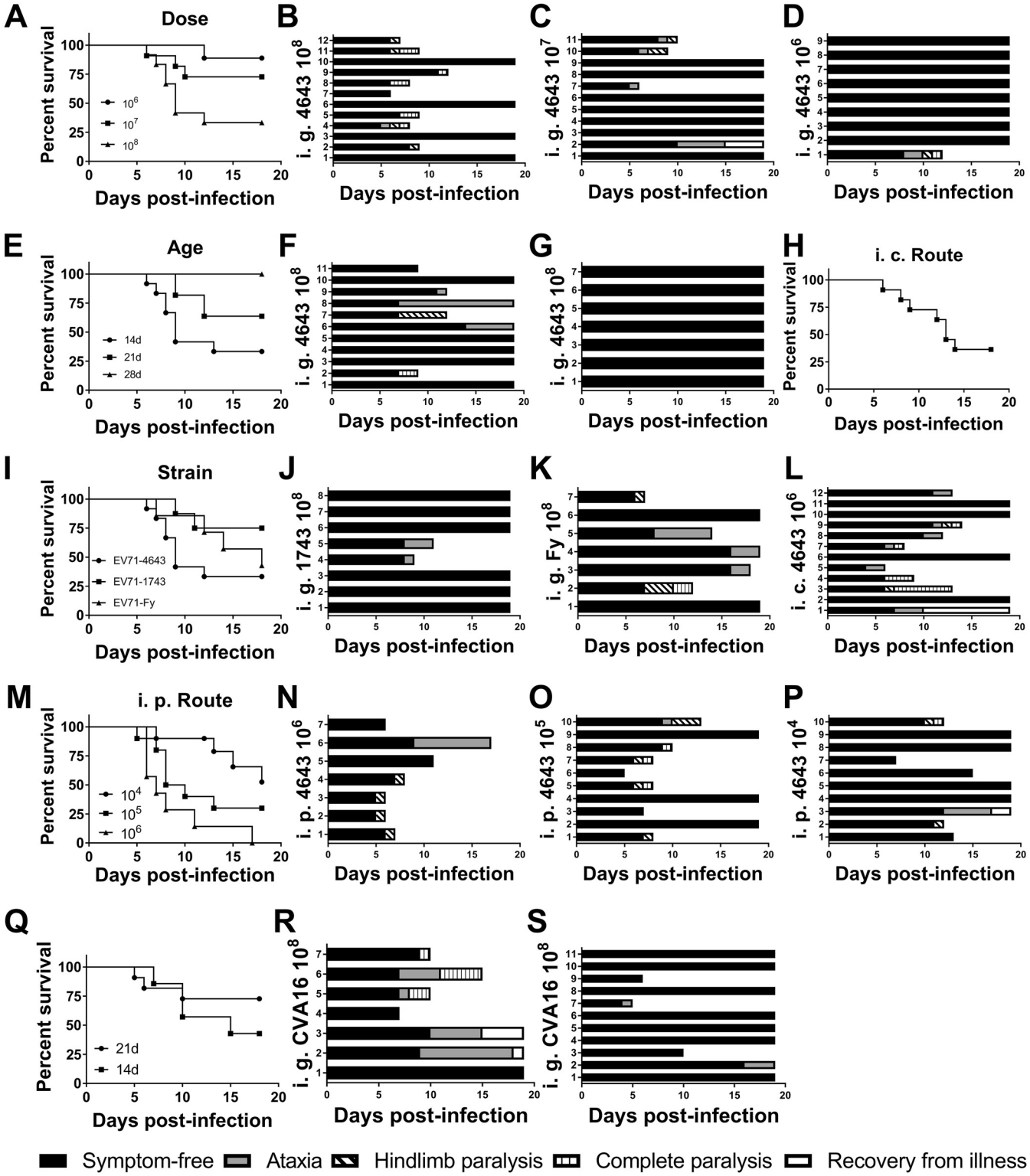

FIG 2 Tg mice are susceptible to oral EV71 and CVA16 infection. (A to P) Tg mice were infected with EV71 under different conditions, such as viral doses (A to D), mouse ages (E, B, F, and G), clinical isolates (I, B, J, and K), and inoculation routes (intraperitoneal [i.p.] route [M to P] and intracerebral [i.c.] route [H and L]). Survival curves (A, E, H, I, and M) and neurological signs (B to D, F, G, J to L, and N to P) are shown. For the charts showing neurological signs, the numbers alongside the ordinate axis refer to the identification numbers of mice within the particular experimental group. (A to D) For testing the effect of viral dosage (A), Tg mice were intragastrically (i.g.) infected with 1×10^6 PFU (D), 1×10^7 PFU (C), or 1×10^8 PFU (B) of the EV71-4643 strain at the age of 14 days. (E to G) Tg mice were i.g. infected with 1×10^8 PFU of the EV71-4643 strain (E) at the age of 14 days (B), 21 days (F), or 28 days (G). (H and L) Tg mice were i.c. infected with 1×10^6 PFU of the EV71-4643 strain at the age of 1 year. (I to K) Tg mice were i.g. infected (I) with 1×10^8 PFU of the EV71-4643 (B), EV71-1743 (J), or EV71-Fy (K) strain at the age of 14 days. (M to P) Tg mice were intraperitoneally (i.p.) infected (M) with 1×10^4 PFU (P), 1×10^5 PFU (O), or 1×10^6 PFU (N) of

(Continued on next page)

eosinophilic cytoplasm were observed among the ventral motor neurons of the thoracic spinal cord. The dorsal sensory neurons were affected to a lesser extent. The severity of the spinal cord lesions was aggravated in moribund mice. Mild focal neuronophagia occurred in the vicinity of dying neurons. For most of the infected mice, there were focal areas of necrosis in skeletal muscle. Apart from these regions, the sarcomere structure of the muscle fibers was largely intact. Myocytolysis and necrosis occurred in the skeletal muscle of moribund mice. Histologically, this was characterized by sarcoplasmic fragmentation, granular degeneration, and loss of striation. At the hind-limb paw, there were focal peridigital necrotic areas with accumulation of eosinophilic amorphous materials. Necrotic sarcoplasmic debris was also present nearby (Fig. 3A).

To validate viral replication in tissues of infected Tg mice, we inoculated 2-week-old Tg and non-Tg mice via the i.g. route; harvested various tissues on days 3, 5, and 7 after infection, and quantified the virus. EV71 was detected in portions of gastrointestinal (GI) tract, including stomach, anterior and posterior small intestine, and colon, in Tg and non-Tg mice on day 3 postinfection (p.i.) (Fig. 3B). For the infected non-Tg mice, the virus was not detectable afterward, suggesting that intragastrically delivered virus may remain stable within the GI tract for only a few days after inoculation and be cleared later. For the infected Tg mice, the EV71 titer decreased significantly in stomach and colon on day 5 p.i. but increased again on day 7 p.i. (Fig. 3B). The EV71 titer in small intestine remained elevated for the rest of the study period (Fig. 3B). The virus became detectable in the brains and spinal cords of infected Tg mice on day 5 p.i., and the viral titer increased further thereafter (Fig. 3B). On the contrary, it could not be detected in the same tissues of non-Tg mice throughout the study period. EV71 could be detected in skeletal muscle of some infected Tg mice (Fig. 3B). For other tissues, such as heart, liver, spleen, and kidney, EV71 was undetectable in the infected Tg mice. Again, EV71 was not detected in the corresponding tissues of the non-Tg mice.

Increases in cytokines in the brains of EV71-infected Tg mice. Cytokines are dysregulated in the CNS in EV71-infected patients, which is probably involved in viral pathogenesis (27). We evaluated the changes in the expression of proinflammatory cytokines in the brains of orally infected Tg mice. Tg and non-Tg mice were inoculated i.g. with the virus, and brains were harvested from non-Tg mice, Tg mice with neurological symptoms (Tg/Symp), and Tg mice without such symptoms (Tg/No Symp) at 7 days p.i. RNA was extracted for reverse transcription-quantitative PCR (RT-qPCR) analysis of the transcripts of cytokines. As shown in Fig. 4, expression levels of genes encoding interferon gamma (IFN-γ), interleukin-1β (IL-1β), chemokine (C-X-C motif) ligand 9 (CXCL9), CXCL10, chemokine (C-C motif) ligand 2 (CCL2), and IL-6 increased in the Tg/Symp group but not in the Tg/No Symp and non-Tg groups. These findings suggest that EV71 infection induces the expression of proinflammatory cytokines in the brain.

Activation of microglia in the brains of EV71-infected Tg mice. Microglial activation plays an important role in neuroinflammation (28). Ionized calcium binding adaptor molecule 1 (Iba1) is considered a microglia-specific marker and is upregulated in activated microglia (29). To examine whether microglia are activated in EV71-infected Tg mice, we immunohistochemically detected Iba1 expression in brain sections collected from Tg and non-Tg mice 6 days after intragastric inoculation with virus. The microglia that were strongly Iba1 positive were widely distributed across the brainstem, hypothalamus, hippocampus, and cerebral cortex of the infected Tg mice. These cells took bushy and amoeboid forms characteristic of activated microglia (Fig. 5A). In contrast, microglia in the same tissues of infected non-Tg mice were very weakly stained for Iba1, and these cells took a ramified form (Fig. 5A). The "ramified" microglia

FIG 2 Legend (Continued)
the EV71-4643 strain at the age of 14 days. Survival rates and clinical symptoms were recorded daily for 18 consecutive days. (Q to S) Tg mice are also susceptible to oral CVA16 infection. Tg mice were i.g. infected with 1×10^8 PFU of CVA16 at the ages of 14 days (Q and R) and 21 days (Q and S). Survival rates (Q) and clinical symptoms (R and S) were recorded daily for 18 consecutive days.

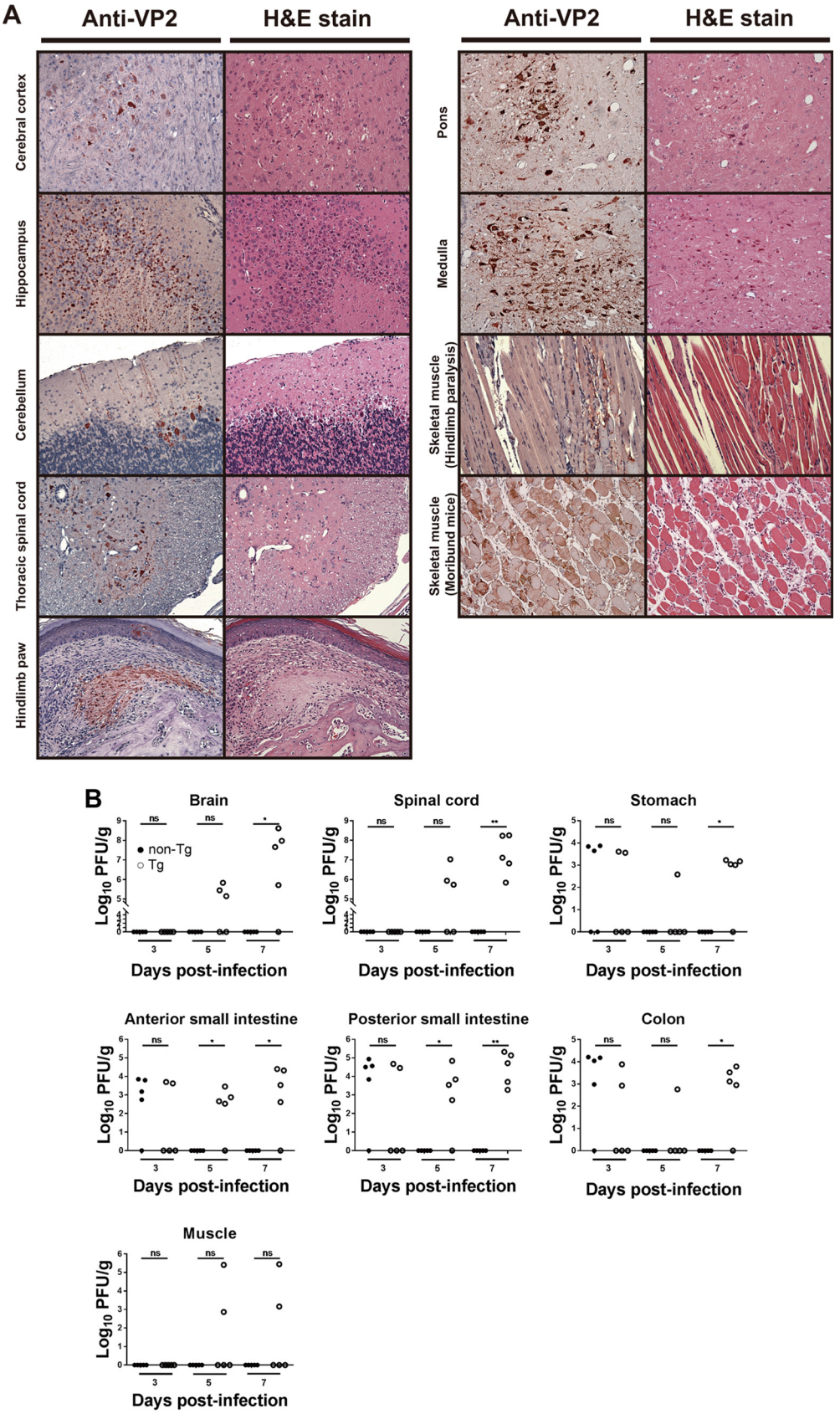

FIG 3 Replication of EV71 in orally infected Tg mice. (A) Histopathological changes and expression of EV71 VP2 protein in infected mice. Two-week-old Tg mice were inoculated i.g. with the EV71-4643 strain and euthanized at 6 days

(Continued on next page)

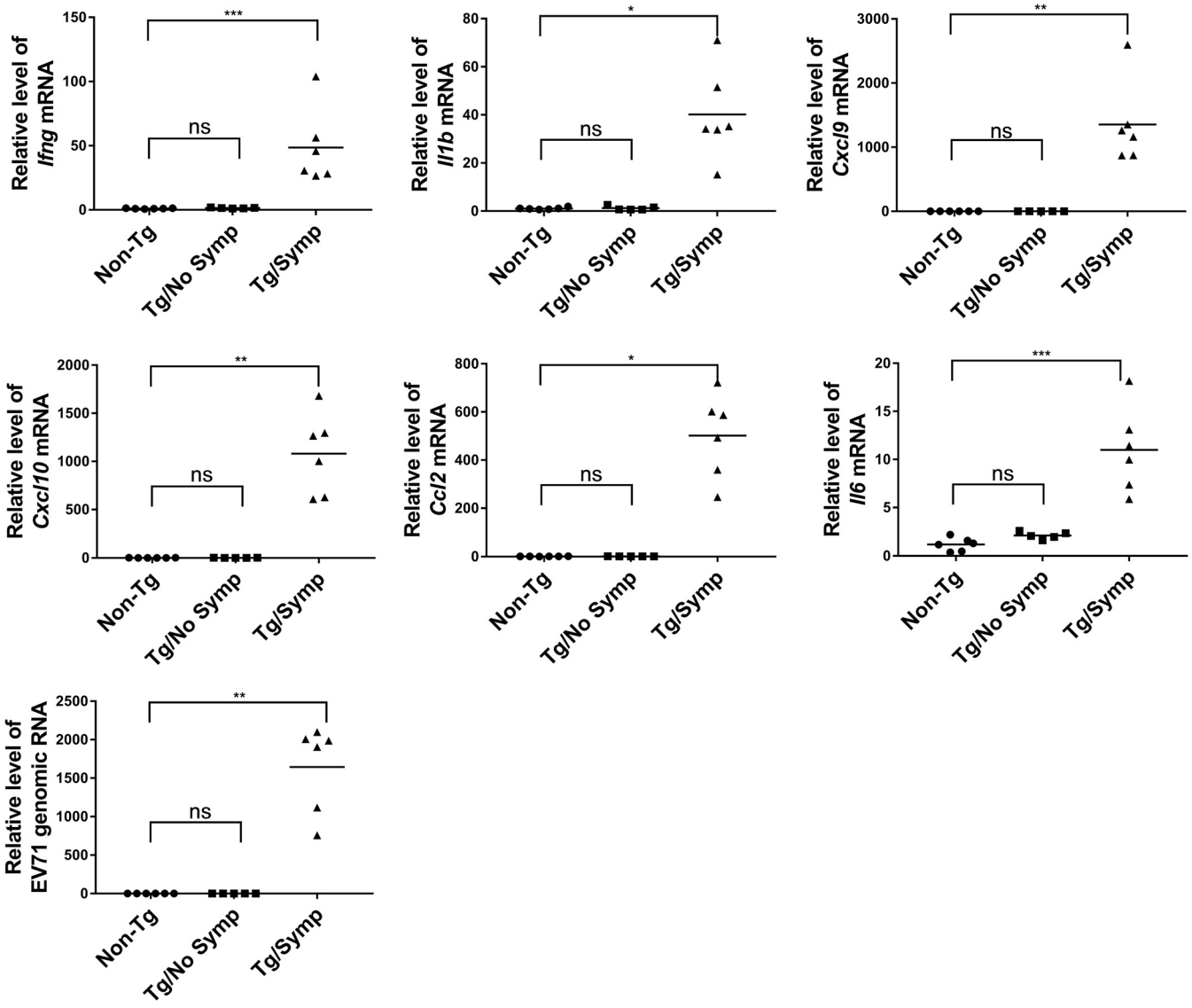

FIG 4 Expression of proinflammatory cytokines in the brains of EV71-infected mice. Tg ($n = 11$) and non-Tg ($n = 5$) (circles) mice were infected i.g. with 1×10^8 PFU of the EV71-4643 strain at the age of 14 days and sacrificed at 7 days p.i. Tg mice were divided into mice without neurological symptoms (Tg/No Symp) (squares) ($n = 5$) and those with symptoms (Tg/Symp) (triangles) ($n = 6$). Brains were isolated from these mice for total RNA extraction. Levels of *Ifng*, *Il1b*, *Cxcl9*, *Cxcl10*, *Ccl2*, and *Il6* mRNAs and of EV71 genomic RNA were determined by RT-qPCR. Data are expressed as fold changes relative to the levels in non-Tg mice. ns, not significant; *, $P < 0.05$; **, $P < 0.01$; ***, $P < 0.001$ (versus non-Tg mice [by a Kruskal-Wallis test with Dunn's multiple-comparison test]).

are considered to be in a resting state. These findings suggest that EV71 infection causes widespread microglia activation. To further characterize microglia activation in the infected Tg mice, we isolated microglia from brains of these mice. It was found that the number of microglia in Tg mice was higher than those in non-Tg mice and Tg mice

FIG 3 Legend (Continued)
postinfection. (Left) Cerebral cortex, hippocampus, cerebellum, thoracic spinal cord, pons, medulla, skeletal muscle (mice with hind-limb paralysis and moribund mice with complete paralysis), and hind-limb paw of Tg mice were retrieved for sample processing, IHC staining with the anti-EV71 VP2 antibody, and hematoxylin counterstaining. (Right) In parallel, sections were stained with H&E. Original magnification, ×200. A representative result out of six experiments is shown. (B) Viral titers in various parts of the CNS and GI tract and in skeletal muscle of infected mice. Two-week-old Tg and non-Tg mice were infected i.g. with 1×10^8 PFU of the EV71-4643 strain and euthanized at the indicated times. Brains and GI tracts were collected and dissected into parts, as indicated in the figure. The anterior small intestine includes the duodenum and parts of the jejunum, while the posterior small intestine includes parts of the jejunum and ileum. Viral titers were determined using a plaque-forming assay and are expressed as log PFU per gram of tissue. ns, not significant; *, $P < 0.05$; **, $P < 0.01$ (versus non-Tg mice [by a Mann-Whitney test]).

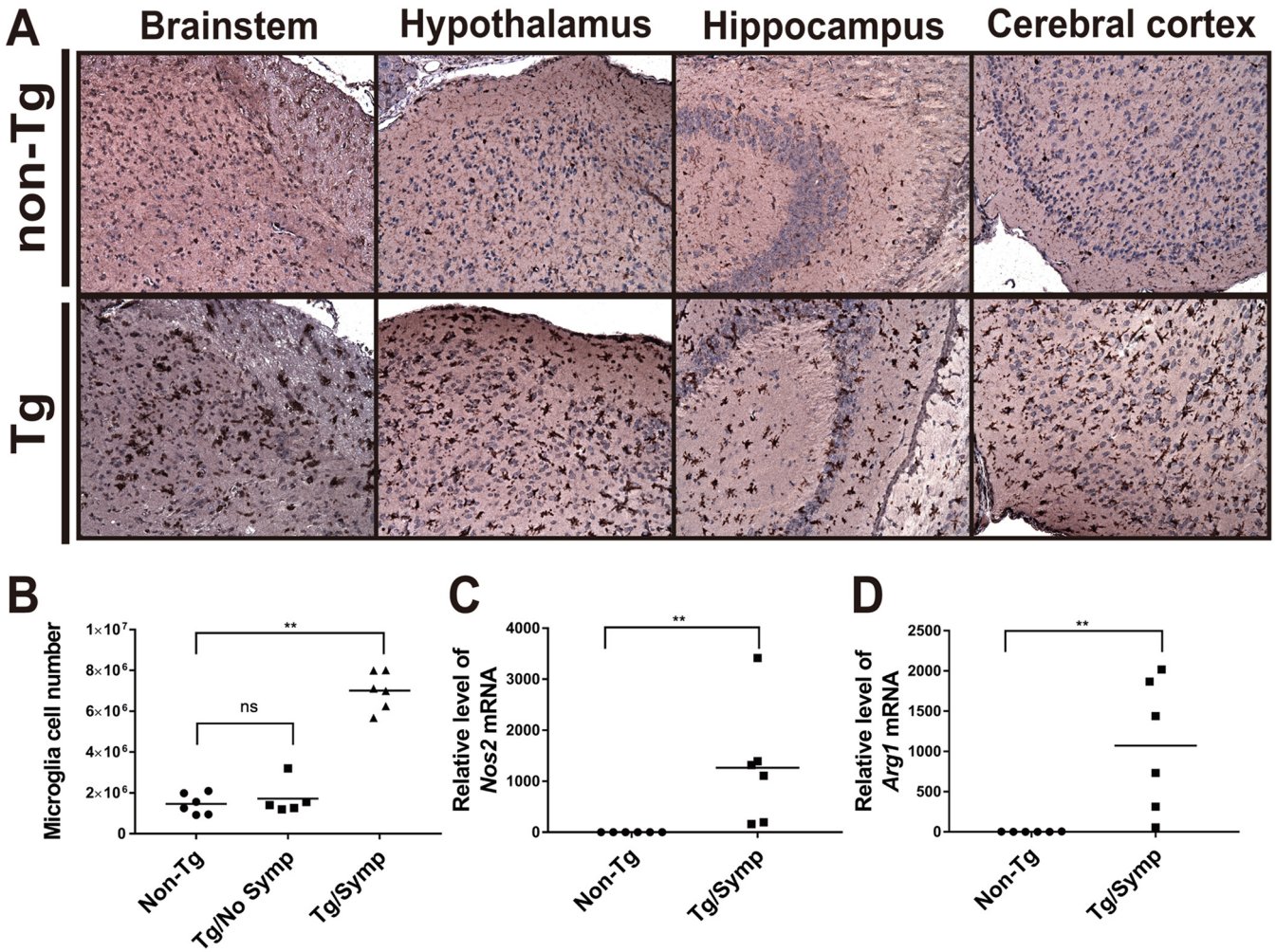

FIG 5 Microglial activation in infected Tg mice. (A) IHC analysis of activated microglia in various parts of the brains of infected Tg mice. Two-week-old Tg and non-Tg mice were inoculated i.g. with 1×10^8 PFU of the EV71-4643 strain and sacrificed at 6 days p.i. Brains were retrieved for sample processing, IHC staining with the anti-Iba1 antibody, and hematoxylin counterstaining. Original magnification, ×200. (B) Increases in microglia numbers in infected Tg mice with symptoms. Tg and non-Tg ($n = 6$) (circles) mice were infected i.g. with 1×10^8 PFU of the EV71-4643 strain at the age of 14 days and sacrificed at 7 days p.i. Tg mice were divided into mice without neurological symptoms (Tg/No Symp) (squares) ($n = 5$) and those with symptoms (Tg/Symp) (triangles) ($n = 6$). Brains were isolated from these mice, and microglia were purified by Percoll gradient centrifugation. Microglia numbers were determined by hemocytometer counting. ns, not significant; **, $P < 0.01$ (versus non-Tg mice [by a Kruskal-Wallis test with Dunn's multiple-comparison test]). (C and D) Microglia in the Tg/Symp and non-Tg groups were isolated as described above for panel B. Total RNA was purified and subjected to RT-qPCR analysis of the expression levels of the M1 activation marker *Nos2* (C) and the M2 activation marker *Arg1* (D). Data are expressed as fold changes relative to the value for non-Tg mice. **, $P < 0.01$ (versus non-Tg mice [by a Mann-Whitney test]).

without any neurological symptoms (Tg/No Symp) (Fig. 5B). There was not any difference in microglial numbers between the latter two groups. Activated microglia can be conventionally classified as classically activated (proinflammatory) M1 or alternatively activated (anti-inflammatory) M2 cells (30). Nitric oxide synthase 2 (*Nos2*) and arginase (*Arg1*) are markers of M1 and M2 cells (30). To test if microglia in the infected Tg mice are polarized toward an M1 or M2 phenotype, we quantified the levels of *Nos2* and *Arg1* transcripts. Expression levels of both the *Nos2* and *Arg1* genes increased in microglia of Tg/Symp mice but not in those of non-Tg mice (Fig. 5C and D). These findings suggest that both M1 and M2 microglia are present in EV71-infected mice.

It is speculative whether microglial activation represents an antiviral response in the infected Tg mice. To examine such a possibility, we treated the brain slices with clodronate liposome to deplete microglia (31) and examined the effect of microglia depletion on EV71 infection. The brains of Tg mice were sectioned into brain slices, which were cultured with clodronate liposome for 48 h and infected with virus. The

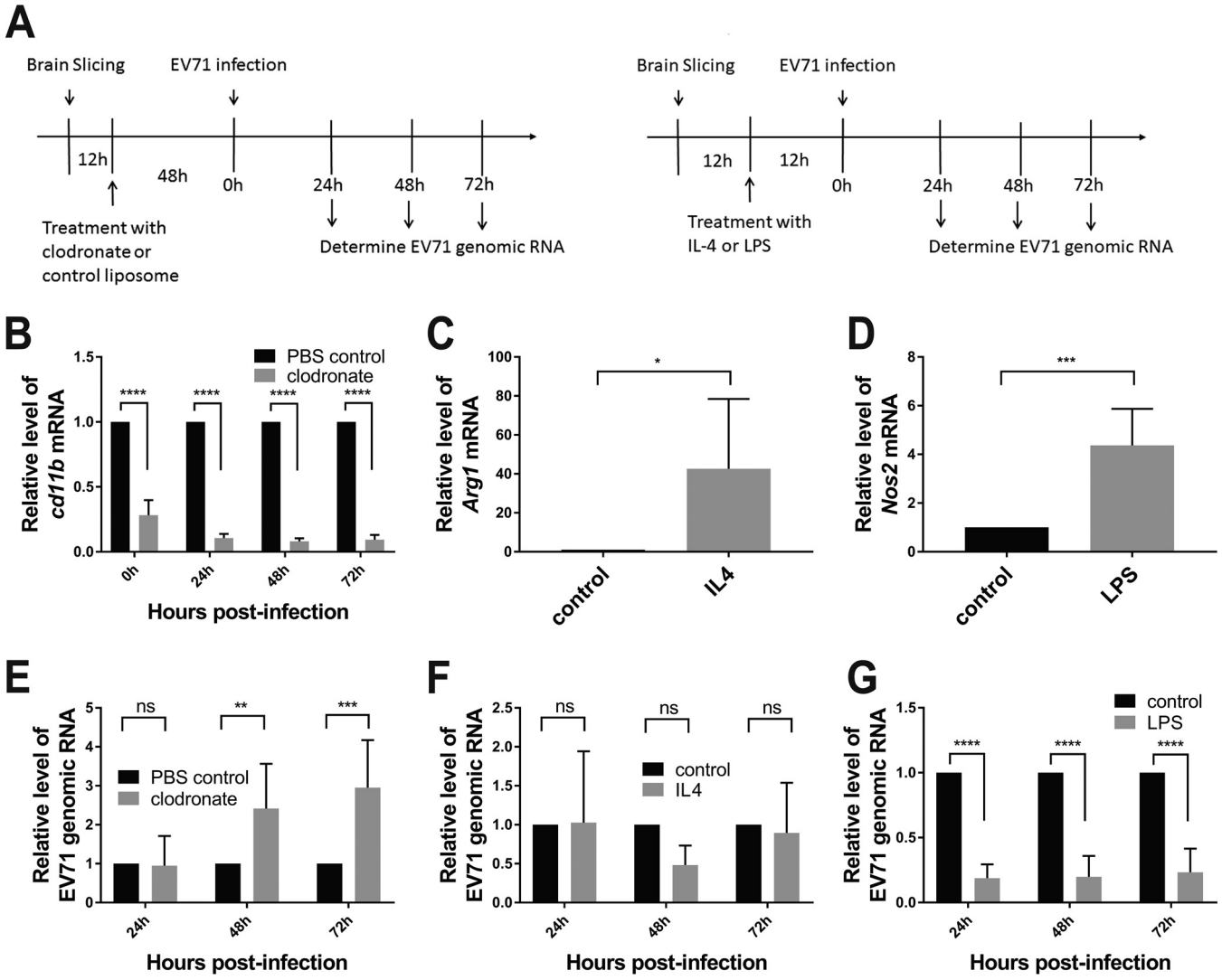

FIG 6 Antiviral response of activated microglia. (A) Brain slices were prepared from Tg mice. The workflow of clodronate treatment of brain slices (left) and induction of microglial polarization in these slices (right) is shown. (B and E) Twelve hours after brain slicing, the slices were treated with clodronate or control liposome for 48 h prior to infection with 10^4 PFU of the EV71-4643 strain per slice (A, left). *Cd11b* mRNA (B) and EV71 genomic RNA (E) were quantified at the indicated times p.i. by RT-qPCR. Data are expressed as fold changes relative to the value for control treatment. Data are means ± SD ($n = 6$). ns, not significant; **, $P < 0.01$; ***, $P < 0.001$; ****, $P < 0.0001$ (versus control treatment). (C, D, F, and G) Twelve hours after brain slicing, the slices were treated with IL-4 or LPS for 12 h (A, right). (C and D) The change in the level of *Arg1* (C) or *Nos2* (D) mRNA in response to IL-4 (C) or LPS (D) treatment was determined using RT-qPCR. (E and F) IL-4 (F)- and LPS (G)-treated brain slices were infected with 10^4 PFU of the EV71-4643 strain per slice, and the levels of EV71 genomic RNA were quantified at the indicated times p.i. by RT-qPCR. Data are expressed as fold changes relative to the value for control treatment. Data are means ± SD ($n = 6$). ns, not significant; *, $P < 0.05$; ***, $P < 0.001$; ****, $P < 0.0001$ (versus control treatment [by two-way ANOVA with Sidak's multiple-comparison test and by Student's *t* test]).

brain slices were extracted at various time points for quantification of EV71 RNA (Fig. 6A). Downregulation of the *Cd11b* transcript was indicative of specific depletion of microglia. Forty-eight-hour treatment of brain slices with clodronate liposome caused a >70% reduction in *Cd11b* expression (Fig. 6B). This was associated with significant increases in EV71 genomic RNA levels at 48 and 72 h p.i. (Fig. 6E). These findings suggest that microglia may exert an antiviral effect against EV71 infection.

To study if M1 or M2 cells are involved in antiviral immunity, we preferentially activated microglia to acquire the M1 or M2 phenotype and studied the consequence for EV71 infection. Lipopolysaccharide (LPS) is known to activate microglia toward M1 cells (32, 33); IL-4 causes microglial polarization toward the M2 state (32). The brain slices from Tg mice were treated with LPS or IL-4 and subsequently infected with virus. EV71 genomic RNA was quantified at various time points after infection. Treatment with

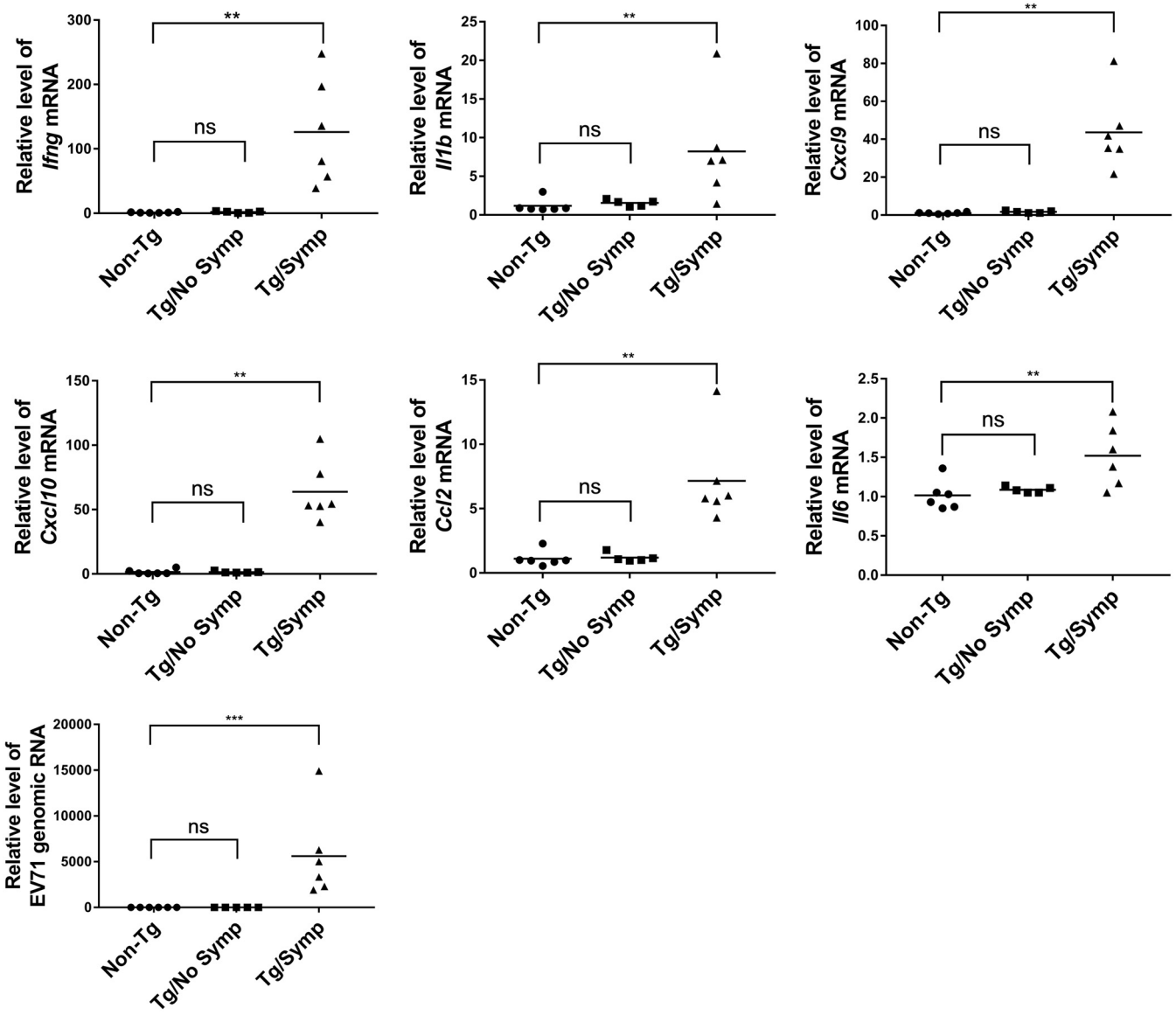

FIG 7 Expression of proinflammatory cytokines in microglia from EV71-infected Tg mice. Two-week-old Tg and non-Tg ($n = 6$) (circles) mice were inoculated i.g. with 1×10^8 PFU of the EV71-4643 strain and sacrificed at 7 days p.i. Tg mice were divided into mice without neurological symptoms (Tg/No Symp) (squares) ($n = 5$) and those with symptoms (Tg/Symp) (triangles) ($n = 6$). Brains were isolated from these mice, and microglia were purified by Percoll gradient centrifugation. Total RNA from microglia was purified for RT-qPCR analysis of the levels of *Ifng*, *Il1b*, *Cxcl9*, *Cxcl10*, *Ccl2*, and *Il6* mRNAs and of EV71 genomic RNA. Data are expressed as fold changes relative to the values for microglia from non-Tg mice. ns, not significant; **, $P < 0.01$; ***, $P < 0.001$ (versus non-Tg mice [by a Kruskal-Wallis test with Dunn's multiple-comparison test]).

IL-4 and LPS increased *Arg1* and *Nos2* transcripts, respectively (Fig. 6C and D), which was consistent with the treatment-induced microglial polarization toward M2 and M1 states. LPS treatment but not IL-4 treatment significantly reduced the level of EV71 genomic RNA (Fig. 6F and G). These findings suggest that M1 microglia play an antiviral role against EV71 replication.

To study if activated microglia are a source of cytokines in EV71-infected Tg mice, we isolated microglia from orally infected Tg mice at 7 days p.i. and extracted RNA for determination of the transcript levels of cytokines. As shown in Fig. 7, the expression levels of *Ifng*, *Il1b*, *Cxcl9*, *Cxcl10*, *Ccl2*, and *Il6* were significantly elevated in Tg/Symp mice, compared to those in non-Tg and Tg/No Symp mice. The latter two groups did not show any difference in the expression of these cytokines. These findings suggest that EV71 infection activates microglia to upregulate their cytokine production. Addi-

tionally, EV71 genomic RNA was detected exclusively in the microglia isolated from the infected Tg mice with neurological symptoms (Fig. 7), implying that microglia are susceptible to EV71 infection.

DISCUSSION

Here, we established a new transgenic mouse expressing a chimeric mSCARB2/hSCARB2 protein, the expression of which conferred susceptibility to intragastric infection with clinical EV71 strains of the B4, C2, and C4 genotypes. The infected transgenic mice displayed neurological symptoms that resembled those associated with severe cases of human infection (Fig. 2). Our model largely simulated the natural route of EV71 infection and disease manifestation in patients. IHC staining for the EV71 protein VP2 and/or viral quantification assays revealed viral replication in CNS tissues and the gastrointestinal tract (Fig. 3), which is suggestive of EV71 replication in various tissues. Microglia were activated in the infected transgenic model, and M1 cells exerted an antiviral effect against EV71 infection.

There are similarities in clinical features between human infection and our mouse model. Tg mice that were infected with EV71 via the i.g., i.p., and i.c. routes developed neurological symptoms. The neurovirulence of EV71 was associated with histopathologic changes and the expression of VP2 protein in cerebral cortex, cerebellum, brainstem, and spinal cord. Purkinje cells (in cerebellum) stained positive for VP2. These neuropathological features were highly similar to those of deceased patients with severe EV71 infection (34, 35) and to those of cynomolgus and rhesus monkeys (15, 36). Another similarity to human infection is the route of viral transmission. EV71 is mainly transmitted via the fecal-oral route (1). It is conceivable that EV71 infects and replicates in the GI tract (37), passes into the bloodstream, and invades the CNS via the blood-brain barrier, or it spreads to the CNS via retrograde axonal transport along peripheral or cranial nerves (38, 39). Unlike other murine infection models (25, 26), our Tg mice are highly susceptible to intragastric infection with EV71. A low level of EV71 replication occurred in various parts of the GI tract (Fig. 3), consistent with the notion that the GI tract may be a primary replication site.

Apparently, there are parallels between histopathological changes in skeletal muscle between human infection and Tg mice. The skeletal muscle of a deceased EV71 patient showed atrophic changes or focal necrosis (35), which is mild compared with the muscle specimens from infected mice. The skeletal muscles of the neonatal mice that had been intraperitoneally inoculated with EV71 displayed severe myositis and degenerative changes (35, 40). An EV71-infected NOD/SCID neonate had extensive degenerative changes in muscle, which showed focal areas of VP1 expression (22). The skeletal muscles of our infected Tg mice were affected to a lesser extent than what was observed in other mouse infection models (20, 25, 35, 40). The Tg mice with hind-limb paralysis had focal areas of necrosis in skeletal muscle, and VP2 expression was restricted to localized areas. EV71 replicated to a relatively low level in skeletal muscle, compared with that in neural tissues. Only in expiring mice did skeletal muscle exhibit severe degenerative changes. These findings suggest that the histopathological changes in skeletal muscles of the infected Tg mice up to the stage of hind-limb paralysis somewhat resemble those observed in EV71 patients. There are differences between the Tg mouse model and human infection. The infected Tg mice did not show a papulovesicular rash on extremities and oral ulcers, both of which are common clinical features of EV71 infection. However, observed that EV71 replicated in the dermis of the paw of a few mice.

Our finding implies the existence of an intricate mechanism that governs viral susceptibility and tissue tropism. Another transgenic mouse that ubiquitously expresses hSCARB2 under the control of the EF-1α promoter was susceptible to subcutaneous EV71 inoculation up to the age of 2 weeks. Viral replication, as indicated by the level of RNA, took place predominantly in muscle and skin and to a lesser extent in brainstem, intestine, and spinal cord (25). Additionally, Liou et al. derived a transgenic mouse that expresses hSCARB2 under the control of a *SCARB2* promoter. The neonates of this

transgenic line displayed low susceptibility to intraperitoneal viral inoculation (41). Furthermore, Fujii et al. used a human *SCARB2* gene-containing BAC to establish a transgenic mouse, which could be effectively infected with the Isehara strain via the i.c., i.v., and i.p. routes (26). Nonetheless, this transgenic mouse was slightly susceptible to i.g. inoculation. The predominant sites of viral replication included pons, medulla, spinal cord, and skeletal muscle. In comparison, our Tg mice could be effectively infected via all the routes tested, which are the i.g., i.p., and i.c. routes. EV71 replication was detected in the CNS and, to a lesser extent, in various parts of the GI tract and skeletal muscles. It is true that these transgenic lines as well as our Tg mouse express the hSCARB2 protein (or protein part) that is essential for viral entry. Even so, these mice exhibit different susceptibilities to EV71, and the EV71 replication sites vary among these models. Moreover, the tissue expression pattern of hSCARB2 does not correlate with tissue tropism. The expression level of the mSCARB2/hSCARB2 protein in Tg mice, regulated in a way similar to that of endogenous protein, was high in tissues such as heart, liver, and spleen. Despite this, EV71 did not efficiently infect and replicate in these tissues. It is likely that other factors in addition to hSCARB2 determine viral susceptibility and tissue tropism. Antiviral immunity, the availability of factors involved in innate immunity, the expression of certain antiviral microRNAs (miRNAs), and the presence of host factors essential for viral replication are among such determinants (42). Moreover, the murine microbiota may affect viral susceptibility and severity of infection (43).

Age is an important factor for human EV71 infection (44). Animal age appears to be related to viral susceptibility (22, 24, 25). Tg mice up to the age of 3 weeks were susceptible to oral EV71 infection. On the other hand, intracerebral inoculation still led to successful infection up to the age of 1 year. Likewise, Fujii et al. reported that mice transgenic for the *SCARB2*-containing BAC displayed susceptibility to viral inoculation via the i.v. and i.p. routes up to the age of 2 weeks, while mice aged 18 weeks were susceptible via the i.c. route (26). These findings suggest the presence of host factors that restrict infection through the mucosa of the GI tract. Intestinal antiviral immunity and epithelial tolerance are probably such factors and may change in an age-dependent manner (45). Dynamic interactions between gut microbiota and mucosal immunity may further shape antiviral immunity (46). However, there is much complexity in this issue, as immunodeficient mice, for instance, AG129 mice and NOD/SCID mice, showed age-dependent changes in their susceptibility to EV71 (22, 24). It remains to be investigated what host factors determine the relationship between age and viral susceptibility.

Another point is noteworthy. Although CVA16 is generally associated with mild symptoms, it has been reported to cause neurological complications (47–49). Infected Tg mice develop neurological symptoms after intragastric CVA16 infection and present a model for neuropathogenesis associated with CVA16 infection.

Microglia act as a first line of defense against pathogens in the CNS and become activated in response to tissue injury or infection (50). They are broadly classified into proinflammatory M1 and alternatively activated M2 cells. M1-polarized microglia produce proinflammatory cytokines such as IL-1β, IL-6, and tumor necrosis factor alpha (TNF-α); the chemokine CCL2; reactive oxygen species; and nitric oxide. M2-polarized cells are anti-inflammatory in nature and express IL-10, transforming growth factor β, and extracellular matrix. Both M1 and M2 microglia may be present in the brains of infected Tg mice. Experimental depletion of microglia through clodronate treatment enhanced EV71 replication. In contrast, LPS-induced M1 polarization was inhibitory to EV71 replication. This is consistent with the increased expression of IL-1β and IFN-γ in activated microglia. Both of these cytokines play pivotal roles in antiviral immunity (51). It is likely that activated M1 microglia exert an antiviral effect against EV71 infection. The immune response, if dysregulated, can be pathogenic. The heightened activation of microglia, together with the activation of astrocytes and neurons, may lead to a cytokine storm, a term coined for temporary and spatially dysregulated cytokine release. It has been postulated that inappropriately regulated cytokine secretion con-

tributes to EV71-induced brainstem encephalitis (27). An alternative but nonexclusive view is that reactive astrocytes may cause neurotoxicity (52). Activated microglia secrete factors to induce the formation of neuroinflammatory A1 astrocytes (53), which may release neurotoxic substances, such as reactive oxygen species and glutamate, and even proinflammatory cytokines (54). Neurotoxic substances can reduce neuronal activity and synaptic connectivity and cause death of neurons. Regardless of the mechanisms, the widespread microglial activation in the CNS of EV71-infected Tg mice may cause neural dysfunction.

In conclusion, we established a BAC transgenic mouse model of EV71 infection that simulates the natural route of human EV71 infection. Our model provides an opportunity to study enteroviral pathogenesis, the host factors thereby involved, as well as antiviral immunity. Moreover, this murine model can be applied for assessment of the efficacies of EV71 vaccines and antiviral therapeutics.

MATERIALS AND METHODS

Cells and viruses. Human rhabdomyosarcoma (RD) cells (ATCC CCL-136) were cultured in Dulbecco's modified Eagle medium (DMEM; Thermo Fisher Scientific, Waltham, MA, USA), supplemented with 10% fetal bovine serum (FBS), 2 mM L-glutamine, 0.1 mM nonessential amino acid (NEAA; Gibco), 100 U/ml penicillin, and 0.1 mg/ml streptomycin, in a humidified atmosphere of 5% CO_2 at 37°C. Three clinically relevant EV71 strains, EV71/TW/4643/98 (EV71-4643) (C2 genogroup), EV71 Fuyang (EV71-Fy) (C4 genogroup), and EV71/TW/1743/98 (EV71-1743) (B4 genogroup), were used in this study. These EV71 strains and a clinical isolate of coxsackievirus A16 (CVA16) were propagated in RD cells as previously described (55). The clinical isolate of CVA16 was kindly provided by the Chang Gung University Research Center for Emerging Viral Infections (RCEVI).

Virus quantification. Virus titer was determined by a PFU assay as previously described (56). Briefly, RD cells were seeded in 6-well plates, infected with serial dilutions of the virus suspension, overlaid with 0.3% agarose in DMEM containing 2% FBS, and incubated at 37°C for 3 days. After the formation of plaques, the cell monolayer was fixed in 10% formalin and stained with 0.5% crystal violet. For titration of virus in various tissues, mice were sacrificed at 3, 5, and 7 days postinfection, and the brain, spinal cord, stomach, intestine, and colon were harvested. All tissue samples were weighed, frozen in liquid nitrogen, and homogenized in DMEM at 4°C using a Precellys 24 tissue homogenizer and zirconium oxide beads (Bertin Instruments, Montigny-le-Bretonneux, France).

Generation of *Scarb2-SCARB2* BAC Tg mice. The *Scarb2-SCARB2* BAC Tg mouse strain was generated by the genetically modified mouse production service of the National Laboratory Animal Center (Taiwan). For preparation of the transgenic BAC clone, the mouse strain RP23-228N3 was acquired from the Children's Hospital Oakland Research Institute BACPAC Resources Center. A stretch of genomic sequence spanning from exon 3 to exon 12 (between nucleotide [nt] 97847 and nt 115634) was replaced with the corresponding human *SCARB2* cDNA sequence that carries a FLAG tag-coding sequence at the 3′ end using the Red/ET recombination technique (Gene Bridges, Heidelberg, Germany). Briefly, the 50-mer homology regions (HR) (black capital letters in Fig. 1A) flanking the replacement sites in exon 3 and exon 12 were attached to an *rpsL-neo* counterselection cassette by PCR, and the product was electroporated into the BAC host that had been transformed with the Red/ET expression vector. This allows replacement of the genomic sequence with the *rpsL-neo* fragment through homologous recombination. Next, the human *SCARB2* cDNA described above was attached with the same homology arms and electroporated into the BAC host containing the correctly recombined BAC and the Red/ET expression vector. This led to replacement of the counterselection cassette in the BAC through homologous recombination and creation of a humanized transgene (Fig. 1A). The detailed protocol is described in the instruction manual for the counterselection BAC modification kit (Gene Bridges, Heidelberg, Germany). The transgene-containing BAC was purified, PmeI digested, and subjected to pulsed-field gel electrophoresis for isolation of the 107-kb transgene, which was used for pronuclear microinjection. The zygotes were transplanted into pseudopregnant C57BL/6 female mice for generation of C57BL/6J-Tg(*Scarb2-SCARB2*) mice.

Mouse genotyping. For screening of Tg mice, genomic DNA was extracted from mouse tail using an EasyPrep genomic DNA extraction kit (Biotools, Taipei, Taiwan) for PCR analysis. Forward primer BAC-F (5′-TTGTGGCTTAGCATCAGCAGC-3′) and reverse primer BAC-R (5′-TCACCCTGCTCATTTCCCTCTG-3′) were used to amplify a 1,511-bp fragment of the transgene.

Infection of mice. C57BL/6J and Tg mice at the age of 2, 3, or 4 weeks were infected i.g. with the indicated PFU of virus in 30 μl of DMEM. For i.c. and i.p. injections, the indicated PFU of virus in 1 μl and 30 μl of DMEM were injected, respectively. All mice were kept under observation for 18 consecutive days unless they died or were sacrificed due to ethical concern. Body weight and clinical symptoms were recorded daily, and the survival rate was calculated accordingly.

Ethics statement. Animal care and the animal experimental methods described in this study were performed according to the national guide (63). They were approved by the Institutional Animal Care and Use Committee (IACUC) of Chang Gung Memorial Hospital at Linkou (IACUC no. 2012101801 and 2015061103).

Western blot analysis. Expression levels of SCARB2 in different tissues of mice were analyzed by Western blotting as previously described (57). Cerebrum, cerebellum, spinal cord, heart, liver, spleen,

lung, stomach, duodenum, jejunum, ileum, colon, kidney, and skeletal muscle were harvested; snap-frozen in liquid nitrogen; and stored at −80°C. Before analysis, the sample was homogenized in lysis buffer (20 mM Tris-HCl [pH 8], 1% Triton X-100, 137 mM NaCl, 1.5 mM $MgCl_2$, 10% glycerol, 1 mM EGTA, 1 mM NaF, 1 mM Na_3VO_4, 10 mM β-glycerophosphate, 1 mM phenylmethylsulfonyl fluoride, 1 μg/ml leupeptin, 1 μg/ml aprotinin) at 4°C using a Precellys 24 tissue homogenizer and zirconium oxide beads. The protein concentration in the homogenate was determined by a Bradford protein assay (Bio-Rad, Hercules, CA, USA). The tissue homogenates were subjected to immunoblotting with a 1:3,000 dilution of goat anti-SCARB2 antibody (catalog no. AF1966; R&D Systems, Minneapolis, MN, USA) or a 1:3,000 dilution of rabbit anti-FLAG antibody (catalog no. F7425; Sigma-Aldrich). For detection of mSCARB2, a goat anti-SCARB2 antibody (catalog no. sc-25867; Santa Cruz Biotechnology, TX, USA) was used. This was followed by incubation with a 1:10,000 dilution of horseradish peroxidase (HRP)-conjugated donkey anti-goat antibody (catalog no. sc-2056; Santa Cruz Biotechnology, TX, USA) or with a 1:10,000 dilution of HRP-conjugated goat anti-rabbit antibody (catalog no. sc-2004; Santa Cruz Biotechnology, TX, USA) and detection with the ECL detection system. For membrane stripping and antibody reprobing, T-Pro Western blot stripping reagent (catalog no. JB11-K002, T-Pro Biotechnology, Taiwan) was used according to the manufacturer's instructions. The image was captured by either exposure to X-ray film (Fujifilm Super RX-N; Fujifilm Corporation, Tokyo, Japan) (Fig. 1B, top and middle) or the use of an Amersham Imager 600 system (GE Healthcare Life Sciences, Marlborough, MA, USA) (Fig. 1B, bottom).

Histopathological analysis and immunohistochemical staining. Tissues were sectioned, fixed, embedded in paraffin, sliced, and stained with hematoxylin and eosin by the pathology analysis service of the National Laboratory Animal Center (Taiwan). Immunohistochemical staining was performed according to the method of Liang et al. (58). Briefly, the paraffinized tissue sections were dewaxed in xylene and rehydrated through immersion in alcohol of graded concentrations. Antigen was retrieved using Trilogy (Cell Marque, Rocklin, CA, USA), and the endogenous peroxidase activity was quenched with 3% H_2O_2 in methanol. After washing with Tris-buffered saline, the slides were incubated with a 1:1,000 dilution of mouse anti-EV71 (catalog no. MAB979; Millipore, Burlington, MA, USA), a 1:1,000 dilution of rabbit anti-hSCARB2 (catalog no. HPA018014; Sigma-Aldrich, St. Louis, MO, USA), or a 1:1,000 dilution of rabbit anti-Iba1 (catalog no. GTX101495; GeneTex, Irvine, CA, USA) antibody. After primary antibody incubation, EV71 VP2 antigen was detected with the use of a mouse-on-mouse (M.O.M) ImmPRESS HRP (peroxidase) polymer kit (catalog no. MP-2400; Vector Laboratories, Burlingame, CA, USA) and an AEC (3-amino-9-ethyl-carbazole) peroxidase substrate kit (catalog no. SK-4200; Vector Laboratories) according to the manufacturer's instructions, hSCARB2 was detected with the use of an ImmPRESS HRP anti-rabbit IgG (peroxidase) polymer detection kit (catalog no. SK-7401; Vector Laboratories) and an AEC peroxidase substrate kit according to the manufacturer's instructions, and Iba1 was detected using an ImmPRESS HRP anti-rabbit IgG (peroxidase) polymer detection kit and a DAB (3,3′-diaminobenzidine) peroxidase (HRP) substrate kit (catalog no. SK-4100; Vector Laboratories) according to the manufacturer's instructions. The slides were counterstained with GM hematoxylin stain (catalog no. 3008-1; Muto Pure Chemical Co. Ltd., Tokyo, Japan), mounted with VectaMount AQ aqueous mounting medium (catalog no. H-5501; Vector Laboratories), and examined microscopically.

Microglia isolation. Microglia were isolated from murine brain as described previously (59). In brief, mice were euthanized by decapitation. Murine brain was isolated and minced in DMEM–F-12 medium (catalog no. 12500-062; Thermo Fisher Scientific, Waltham, MA, USA) supplemented with 4.5 mg/ml glucose, 100 U/ml penicillin, and 100 μg/ml streptomycin (catalog no. 15140-122; Thermo Fisher Scientific, Waltham, MA, USA). The minced tissue was digested in the same medium, additionally containing 1 mg/ml papain (catalog no. P4762; Sigma-Aldrich), 20 U/ml DNase (catalog no. DN25; Sigma-Aldrich), and 1.2 U/ml dispase II (catalog no. D4693; Sigma-Aldrich), at 37°C for 20 min. Enzymatic activity was quenched with a neutralization medium (DMEM–F-12 medium supplemented with 10% fetal calf serum [FCS], 4.5 mg/ml glucose, 100 U/ml penicillin, and 100 μg/ml streptomycin). The dissociated tissue was centrifuged, and the pellet was washed with serum-free DMEM–F-12 medium. After two washes, the tissue was spun down, and the pellet was pipetted up and down with a large-bore Pasteur pipette to break the tissue clumps. The sample was left undisturbed to allow sedimentation of large clumps, and the upper portion containing dissociated cells was retrieved. This procedure was repeated with a medium-bore and a small-bore pipette, and the cell-containing portions were pooled. The pooled fraction was filtered through a cell strainer (catalog no. 22363547; Fisherbrand), spun down, and washed with serum-free DMEM–F-12 medium once. The cell pellet was resuspended in 4 ml of a 37% isotonic Percoll solution and loaded on top of 4 ml of a 70% isotonic Percoll solution in a 15-ml conical tube. This mixture was overlaid with 4 ml of a 30% isotonic Percoll solution and on its top with 2 ml of Hanks' balanced salt solution (HBSS). The Percoll gradient was centrifuged at 300 × *g* at 18°C for 40 min. About 2.5 ml of the solution at the 70% to 37% interphase was collected, diluted with HBSS, and centrifuged. The cell pellet was washed with HBSS three times and finally resuspended in HBSS for cell counting.

Preparation of brain slice culture and infection. Brain slices were prepared and cultured as described previously (60). Briefly, 7-day-old mice were euthanized by decapitation, and brains were isolated. Cerebrum was separated from cerebellum with a razor blade and glued onto the stage of a vibrating microtome (model 5100mz; Campden Instruments Ltd., UK). The stage was placed in a bath containing ice-cold slicing medium (minimal essential medium [MEM] [catalog no. 41500-018; Thermo Fisher Scientific]–10 mg/ml glucose–1 mM HEPES [pH 7.2]). Eight 300-μm coronal sections with hippocampus/thalamus were obtained. Four brain slices were placed in a 30-mm cell insert (Picmorg50; Merck Millipore, Burlington, MA, USA). The cell insert was placed in a 35-mm culture dish containing plating medium (neurobasal A medium [catalog no. 10888-022; Thermo Fisher Scientific] supplemented with 1× B-27 [catalog no. 17504044; Thermo Fisher Scientific], 10% FBS, 10 mM HEPES, 600 μM

TABLE 1 Primers used in this study

Primer	Sequence (5′–3′)	Reference or source[a]	PrimerBank identification
BAC-F	TTGTGGCTTAGCATCAGCAGC	This study	
BAC-R	TCACCCTGCTCATTTCCCTCTG	This study	
m-GAPDH-F	AGGTCGGTGTGAACGGATTTG	PrimerBank	6679937a1
m-GAPDH-R	TGTAGACCATGTAGTTGAGGTCA	PrimerBank	6679937a1
m-Arg1-F	CTCCAAGCCAAAGTCCTTAGAG	PrimerBank	7106255a1
m-Arg1-R	AGGAGCTGTCATTAGGGACATC	PrimerBank	7106255a1
m-iNOS-F	GTTCTCAGCCCAACAATACAAGA	PrimerBank	6754872a1
m-iNOS-R	GTGGACGGGTCGATGTCAC	PrimerBank	6754872a1
m-Il1b-F	GCAACTGTTCCTGAACTCAACT	PrimerBank	6680415a1
m-Il1b-R	ATCTTTTGGGGTCCGTCAACT	PrimerBank	6680415a1
m-MCP1-F	TTAAAAACCTGGATCGGAACCAA	PrimerBank	6755430a1
m-MCP1-R	GCATTAGCTTCAGATTTACGGGT	PrimerBank	6755430a1
m-Cxcl10-F	CCAAGTGCTGCCGTCATTTTC	PrimerBank	10946576a1
m-Cxcl10-R	GGCTCGCAGGGATGATTTCAA	PrimerBank	10946576a1
m-CXCL9-F	GGAGTTCGAGGAACCCTAGTG	PrimerBank	162287427c1
m-CXCL9-R	GGGATTTGTAGTGGATCGTGC	PrimerBank	162287427c1
m-CD11b-F	TACCGTCTACTACCCATCTGGC	—[b]	
m-CD11b-R	TTGGTGAGCGGGTTCTGG	—[b]	
m-Ifng-F	ATGAACGCTACACACTGCATC	PrimerBank	33468859a1
m-Ifng-R	CCATCCTTTTGCCAGTTCCTC	PrimerBank	33468859a1
4643EV71 VP1_783F	GATACCTCGCCCAATGCGTA	This study	
4643EV71 2A_006R	TTTCCCGAGGGTGGTGATTG	This study	

[a]PrimerBank can be accessed at https://pga.mgh.harvard.edu/primerbank/index.html (61).
[b]The sequences of the m-CD11b-F and m-CD11b-R primers were described previously (62).

GlutaMAX, 400 μM glutamine, 60 U/ml penicillin, 60 μg/ml streptomycin, and 6 U/ml nystatin). The culture was maintained in a humidified incubator with 5% CO_2 at 37°C. The medium was replaced with one containing 5% FBS after 12 h and thereafter replaced with serum-free medium every 2 days. For infection of the brain slice with EV71, 10^4 PFU of EV71-4643 in 20 μl was added to the surface of the brain slice. For IL-4 or lipopolysaccharide (LPS) treatment, recombinant murine IL-4 (at a final concentration of 20 ng/ml) (catalog no. 214-14; PeproTech, NJ, USA) or LPS (at a final concentration of 5 ng/ml) (catalog no. L4516; Sigma-Aldrich) was added to medium supplemented with 5% FBS in the brain slice-containing dish for 12 h. For clodronate liposome treatment, clodronate liposome or phosphate-buffered saline (PBS) liposome (control) (catalog no. CP-005-005; Liposoma, Amsterdam, Netherlands) was added at a final concentration of 0.5 mg/ml to medium supplemented with 5% FBS in the brain slice-containing dish for 48 h. After treatment, medium was exchanged for serum-free medium before viral infection.

Reverse transcription-quantitative PCR. Different tissues, brain slices, or microglia were homogenized in TRIzol (Thermo Fisher Scientific, Waltham, MA, USA), and total RNA was extracted according to the manufacturer's protocol. cDNA was synthesized from total RNA using a RevertAid first-strand cDNA synthesis kit (catalog no. K1622; Thermo Fisher Scientific, Waltham, MA, USA) according to the manufacturer's protocol. The cDNA sample was mixed with SsoFast EvaGreen supermix (catalog no. 172-5201; Bio-Rad, Hercules, CA, USA) in a reaction volume of 10 μl. PCR was performed with the CFX96 Touch real-time PCR detection system (Bio-Rad, Hercules, CA, USA). The primers used in this study are shown in Table 1.

Statistical analyses. All statistical analyses were performed using GraphPad Prism 5 software (GraphPad Software Inc., San Diego, CA, USA). Two-way analysis of variance (ANOVA) with Sidak's multiple-comparison test, two-tailed unpaired Student's *t* test, a Kruskal-Wallis test with Dunn's multiple-comparison test, and a Mann-Whitney test were applied where appropriate. The log rank test was applied to compare the survival rates of different groups of mice. A P value of <0.05 is considered significant.

SUPPLEMENTAL MATERIAL

Supplemental material for this article may be found at https://doi.org/10.1128/JVI.00183-19.

SUPPLEMENTAL FILE 1, AVI file, 1.9 MB.
SUPPLEMENTAL FILE 2, AVI file, 2.2 MB.
SUPPLEMENTAL FILE 3, AVI file, 5 MB.
SUPPLEMENTAL FILE 4, PDF file, 0.02 MB.

ACKNOWLEDGMENTS

The research work was supported, in whole or in part, by grants from Chang Gung Memorial Hospital (BMRP819, BMRP564, CMRPD1F0471, CMRPD1F0472, CMRPD1F0473, CMRPD1H0201, CMRPD1F0511, CMRPD1F0512, and CMRPD1F0513), the Ministry of

Science and Technology in Taiwan (MOST) (MOST 104-2320-B-182-022-MY3, MOST 107-2320-B-182-011-MY3, MOST 104-2320-B-182-017-MY3, and MOST 107-2320-B-182-030), and the Ministry of Education in Taiwan (MOE) (EMRPD1G0251 and EMRPD1H0401). In addition, this work was partly supported by the Research Center for Emerging Viral Infections under the Featured Areas Research Center Program funded within the framework of the Higher Education Sprout Project of the MOE and MOST (MOST 107-3017-F-182-001).

REFERENCES

1. Solomon T, Lewthwaite P, Perera D, Cardosa MJ, McMinn P, Ooi MH. 2010. Virology, epidemiology, pathogenesis, and control of enterovirus 71. Lancet Infect Dis 10:778–790. https://doi.org/10.1016/S1473-3099(10)70194-8.
2. Weng KF, Chen LL, Huang PN, Shih SR. 2010. Neural pathogenesis of enterovirus 71 infection. Microbes Infect 12:505–510. https://doi.org/10.1016/j.micinf.2010.03.006.
3. Yang F, Ren L, Xiong Z, Li J, Xiao Y, Zhao R, He Y, Bu G, Zhou S, Wang J, Qi J. 2009. Enterovirus 71 outbreak in the People's Republic of China in 2008. J Clin Microbiol 47:2351–2352. https://doi.org/10.1128/JCM.00563-09.
4. Yang F, Zhang T, Hu Y, Wang X, Du J, Li Y, Sun S, Sun X, Li Z, Jin Q. 2011. Survey of enterovirus infections from hand, foot and mouth disease outbreak in China, 2009. Virol J 8:508. https://doi.org/10.1186/1743-422X-8-508.
5. Mao LX, Wu B, Bao WX, Han FA, Xu L, Ge QJ, Yang J, Yuan ZH, Miao CH, Huang XX, Zhang C, Xu H. 2010. Epidemiology of hand, foot, and mouth disease and genotype characterization of enterovirus 71 in Jiangsu, China. J Clin Virol 49:100–104. https://doi.org/10.1016/j.jcv.2010.07.009.
6. Yamayoshi S, Yamashita Y, Li J, Hanagata N, Minowa T, Takemura T, Koike S. 2009. Scavenger receptor B2 is a cellular receptor for enterovirus 71. Nat Med 15:798–801. https://doi.org/10.1038/nm.1992.
7. Nishimura Y, Shimojima M, Tano Y, Miyamura T, Wakita T, Shimizu H. 2009. Human P-selectin glycoprotein ligand-1 is a functional receptor for enterovirus 71. Nat Med 15:794–797. https://doi.org/10.1038/nm.1961.
8. Yang SL, Chou YT, Wu CN, Ho MS. 2011. Annexin II binds to capsid protein VP1 of enterovirus 71 and enhances viral infectivity. J Virol 85:11809–11820. https://doi.org/10.1128/JVI.00297-11.
9. Su PY, Wang YF, Huang SW, Lo YC, Wang YH, Wu SR, Shieh DB, Chen SH, Wang JR, Lai MD, Chang CF. 2015. Cell surface nucleolin facilitates enterovirus 71 binding and infection. J Virol 89:4527–4538. https://doi.org/10.1128/JVI.03498-14.
10. Eskelinen EL, Tanaka Y, Saftig P. 2003. At the acidic edge: emerging functions for lysosomal membrane proteins. Trends Cell Biol 13:137–145. https://doi.org/10.1016/S0962-8924(03)00005-9.
11. Yamayoshi S, Iizuka S, Yamashita T, Minagawa H, Mizuta K, Okamoto M, Nishimura H, Sanjoh K, Katsushima N, Itagaki T, Nagai Y, Fujii K, Koike S. 2012. Human SCARB2-dependent infection by coxsackievirus A7, A14, and A16 and enterovirus 71. J Virol 86:5686–5696. https://doi.org/10.1128/JVI.00020-12.
12. Yamayoshi S, Koike S. 2011. Identification of a human SCARB2 region that is important for enterovirus 71 binding and infection. J Virol 85:4937–4946. https://doi.org/10.1128/JVI.02358-10.
13. Hashimoto I, Hagiwara A. 1982. Pathogenicity of a poliomyelitis-like disease in monkeys infected orally with enterovirus 71: a model for human infection. Neuropathol Appl Neurobiol 8:149–156. https://doi.org/10.1111/j.1365-2990.1982.tb00269.x.
14. Chumakov M, Voroshilova M, Shindarov L, Lavrova I, Gracheva L, Koroleva G, Vasilenko S, Brodvarova I, Nikolova M, Gyurova S, Gacheva M, Mitov G, Ninov N, Tsylka E, Robinson I, Frolova M, Bashkirtsev V, Martiyanova L, Rodin V. 1979. Enterovirus 71 isolated from cases of epidemic poliomyelitis-like disease in Bulgaria. Arch Virol 60:329–340. https://doi.org/10.1007/BF01317504.
15. Hashimoto I, Hagiwara A, Kodama H. 1978. Neurovirulence in cynomolgus monkeys of enterovirus 71 isolated from a patient with hand, foot and mouth disease. Arch Virol 56:257–261. https://doi.org/10.1007/BF01317855.
16. Arita M, Shimizu H, Nagata N, Ami Y, Suzaki Y, Sata T, Iwasaki T, Miyamura T. 2005. Temperature-sensitive mutants of enterovirus 71 show attenuation in cynomolgus monkeys. J Gen Virol 86:1391–1401. https://doi.org/10.1099/vir.0.80784-0.
17. Arita M, Nagata N, Iwata N, Ami Y, Suzaki Y, Mizuta K, Iwasaki T, Sata T, Wakita T, Shimizu H. 2007. An attenuated strain of enterovirus 71 belonging to genotype A showed a broad spectrum of antigenicity with attenuated neurovirulence in cynomolgus monkeys. J Virol 81:9386–9395. https://doi.org/10.1128/JVI.02856-06.
18. Yu CK, Chen CC, Chen CL, Wang JR, Liu CC, Yan JJ, Su IJ. 2000. Neutralizing antibody provided protection against enterovirus type 71 lethal challenge in neonatal mice. J Biomed Sci 7:523–528. https://doi.org/10.1007/BF02253368.
19. Wang YF, Chou CT, Lei HY, Liu CC, Wang SM, Yan JJ, Su IJ, Wang JR, Yeh TM, Chen SH, Yu CK. 2004. A mouse-adapted enterovirus 71 strain causes neurological disease in mice after oral infection. J Virol 78:7916–7924. https://doi.org/10.1128/JVI.78.15.7916-7924.2004.
20. Ong KC, Badmanathan M, Devi S, Leong KL, Cardosa MJ, Wong KT. 2008. Pathologic characterization of a murine model of human enterovirus 71 encephalomyelitis. J Neuropathol Exp Neurol 67:532–542. https://doi.org/10.1097/NEN.0b013e31817713e7.
21. Chua BH, Phuektes P, Sanders SA, Nicholls PK, McMinn PC. 2008. The molecular basis of mouse adaptation by human enterovirus 71. J Gen Virol 89:1622–1632. https://doi.org/10.1099/vir.0.83676-0.
22. Liao CC, Liou AT, Chang YS, Wu SY, Chang CS, Lee CK, Kung JT, Tu PH, Yu YY, Lin CY, Lin JS, Shih C. 2014. Immunodeficient mouse models with different disease profiles by in vivo infection with the same clinical isolate of enterovirus 71. J Virol 88:12485–12499. https://doi.org/10.1128/JVI.00692-14.
23. Arita M, Ami Y, Wakita T, Shimizu H. 2008. Cooperative effect of the attenuation determinants derived from poliovirus Sabin 1 strain is essential for attenuation of enterovirus 71 in the NOD/SCID mouse infection model. J Virol 82:1787–1797. https://doi.org/10.1128/JVI.01798-07.
24. Khong WX, Yan B, Yeo H, Tan EL, Lee JJ, Ng JK, Chow VT, Alonso S. 2012. A non-mouse-adapted enterovirus 71 (EV71) strain exhibits neurotropism, causing neurological manifestations in a novel mouse model of EV71 infection. J Virol 86:2121–2131. https://doi.org/10.1128/JVI.06103-11.
25. Lin YW, Yu SL, Shao HY, Lin HY, Liu CC, Hsiao KN, Chitra E, Tsou YL, Chang HW, Sia C, Chong P, Chow YH. 2013. Human SCARB2 transgenic mice as an infectious animal model for enterovirus 71. PLoS One 8:e57591. https://doi.org/10.1371/journal.pone.0057591.
26. Fujii K, Nagata N, Sato Y, Ong KC, Wong KT, Yamayoshi S, Shimanuki M, Shitara H, Taya C, Koike S. 2013. Transgenic mouse model for the study of enterovirus 71 neuropathogenesis. Proc Natl Acad Sci U S A 110:14753–14758. https://doi.org/10.1073/pnas.1217563110.
27. Wang SM, Lei HY, Liu CC. 2012. Cytokine immunopathogenesis of enterovirus 71 brain stem encephalitis. Clin Dev Immunol 2012:876241. https://doi.org/10.1155/2012/876241.
28. Graeber MB, Li W, Rodriguez ML. 2011. Role of microglia in CNS inflammation. FEBS Lett 585:3798–3805. https://doi.org/10.1016/j.febslet.2011.08.033.
29. Imai Y, Kohsaka S. 2002. Intracellular signaling in M-CSF-induced microglia activation: role of Iba1. Glia 40:164–174. https://doi.org/10.1002/glia.10149.
30. Franco R, Fernandez-Suarez D. 2015. Alternatively activated microglia and macrophages in the central nervous system. Prog Neurobiol 131:65–86. https://doi.org/10.1016/j.pneurobio.2015.05.003.
31. Conrady CD, Zheng M, van Rooijen N, Drevets DA, Royer D, Alleman A, Carr DJ. 2013. Microglia and a functional type I IFN pathway are required to counter HSV-1-driven brain lateral ventricle enlargement and encephalitis. J Immunol 190:2807–2817. https://doi.org/10.4049/jimmunol.1203265.
32. Chhor V, Le Charpentier T, Lebon S, Ore MV, Celador IL, Josserand J, Degos V, Jacotot E, Hagberg H, Savman K, Mallard C, Gressens P, Fleiss

B. 2013. Characterization of phenotype markers and neuronotoxic potential of polarised primary microglia in vitro. Brain Behav Immun 32:70–85. https://doi.org/10.1016/j.bbi.2013.02.005.
33. Fu X, Zunich SM, O'Connor JC, Kavelaars A, Dantzer R, Kelley KW. 2010. Central administration of lipopolysaccharide induces depressive-like behavior in vivo and activates brain indoleamine 2,3 dioxygenase in murine organotypic hippocampal slice cultures. J Neuroinflammation 7:43. https://doi.org/10.1186/1742-2094-7-43.
34. Shieh WJ, Jung SM, Hsueh C, Kuo TT, Mounts A, Parashar U, Yang CF, Guarner J, Ksiazek TG, Dawson J, Goldsmith C, Chang GJ, Oberste SM, Pallansch MA, Anderson LJ, Zaki SR. 2001. Pathologic studies of fatal cases in outbreak of hand, foot, and mouth disease, Taiwan. Emerg Infect Dis 7:146–148. https://doi.org/10.3201/eid0701.700146.
35. Yu P, Gao Z, Zong Y, Bao L, Xu L, Deng W, Li F, Lv Q, Gao Z, Xu Y, Yao Y, Qin C. 2014. Histopathological features and distribution of EV71 antigens and SCARB2 in human fatal cases and a mouse model of enterovirus 71 infection. Virus Res 189:121–132. https://doi.org/10.1016/j.virusres.2014.05.006.
36. Zhang Y, Cui W, Liu L, Wang J, Zhao H, Liao Y, Na R, Dong C, Wang L, Xie Z, Gao J, Cui P, Zhang X, Li Q. 2011. Pathogenesis study of enterovirus 71 infection in rhesus monkeys. Lab Invest 91:1337–1350. https://doi.org/10.1038/labinvest.2011.82.
37. Drummond CG, Bolock AM, Ma C, Luke CJ, Good M, Coyne CB. 2017. Enteroviruses infect human enteroids and induce antiviral signaling in a cell lineage-specific manner. Proc Natl Acad Sci U S A 114:1672–1677. https://doi.org/10.1073/pnas.1617363114.
38. Chen CS, Yao YC, Lin SC, Lee YP, Wang YF, Wang JR, Liu CC, Lei HY, Yu CK. 2007. Retrograde axonal transport: a major transmission route of enterovirus 71 in mice. J Virol 81:8996–9003. https://doi.org/10.1128/JVI.00236-07.
39. Tan SH, Ong KC, Wong KT. 2014. Enterovirus 71 can directly infect the brainstem via cranial nerves and infection can be ameliorated by passive immunization. J Neuropathol Exp Neurol 73:999–1008. https://doi.org/10.1097/NEN.0000000000000122.
40. Lin P, Gao L, Huang Y, Chen Q, Shen H. 2015. An enterovirus 71 strain causes skeletal muscle damage in infected mice. Int J Clin Exp Pathol 8:3460–3468.
41. Liou AT, Wu SY, Liao CC, Chang YS, Chang CS, Shih C. 2016. A new animal model containing human SCARB2 and lacking stat-1 is highly susceptible to EV71. Sci Rep 6:31151. https://doi.org/10.1038/srep31151.
42. Lin JY, Shih SR. 2014. Cell and tissue tropism of enterovirus 71 and other enteroviruses infections. J Biomed Sci 21:18. https://doi.org/10.1186/1423-0127-21-18.
43. Robinson CM, Pfeiffer JK. 2014. Viruses and the microbiota. Annu Rev Virol 1:55–69. https://doi.org/10.1146/annurev-virology-031413-085550.
44. Ooi MH, Wong SC, Lewthwaite P, Cardosa MJ, Solomon T. 2010. Clinical features, diagnosis, and management of enterovirus 71. Lancet Neurol 9:1097–1105. https://doi.org/10.1016/S1474-4422(10)70209-X.
45. Tourneur E, Chassin C. 2013. Neonatal immune adaptation of the gut and its role during infections. Clin Dev Immunol 2013:270301. https://doi.org/10.1155/2013/270301.
46. Dzidic M, Boix-Amoros A, Selma-Royo M, Mira A, Collado MC. 2018. Gut microbiota and mucosal immunity in the neonate. Med Sci (Basel) 6:E56. https://doi.org/10.3390/medsci6030056.
47. Goto K, Sanefuji M, Kusuhara K, Nishimura Y, Shimizu H, Kira R, Torisu H, Hara T. 2009. Rhombencephalitis and coxsackievirus A16. Emerg Infect Dis 15:1689–1691. https://doi.org/10.3201/eid1510.090594.
48. Wright HT, Jr, Landing BH, Lennette EH, McAllister RM. 1963. Fatal infection in an infant associated with coxsackie virus group A, type 16. N Engl J Med 268:1041–1044. https://doi.org/10.1056/NEJM196305092681904.
49. Xu W, Liu CF, Yan L, Li JJ, Wang LJ, Qi Y, Cheng RB, Xiong XY. 2012. Distribution of enteroviruses in hospitalized children with hand, foot and mouth disease and relationship between pathogens and nervous system complications. Virol J 9:8. https://doi.org/10.1186/1743-422X-9-8.
50. Kettenmann H, Hanisch UK, Noda M, Verkhratsky A. 2011. Physiology of microglia. Physiol Rev 91:461–553. https://doi.org/10.1152/physrev.00011.2010.
51. Hurgin V, Novick D, Werman A, Dinarello CA, Rubinstein M. 2007. Antiviral and immunoregulatory activities of IFN-gamma depend on constitutively expressed IL-1alpha. Proc Natl Acad Sci U S A 104:5044–5049. https://doi.org/10.1073/pnas.0611608104.
52. Liddelow SA, Barres BA. 2017. Reactive astrocytes: production, function, and therapeutic potential. Immunity 46:957–967. https://doi.org/10.1016/j.immuni.2017.06.006.
53. Liddelow SA, Guttenplan KA, Clarke LE, Bennett FC, Bohlen CJ, Schirmer L, Bennett ML, Munch AE, Chung WS, Peterson TC, Wilton DK, Frouin A, Napier BA, Panicker N, Kumar M, Buckwalter MS, Rowitch DH, Dawson VL, Dawson TM, Stevens B, Barres BA. 2017. Neurotoxic reactive astrocytes are induced by activated microglia. Nature 541:481–487. https://doi.org/10.1038/nature21029.
54. Sofroniew MV, Vinters HV. 2010. Astrocytes: biology and pathology. Acta Neuropathol 119:7–35. https://doi.org/10.1007/s00401-009-0619-8.
55. Chen SG, Leu YL, Cheng ML, Ting SC, Liu CC, Wang SD, Yang CH, Hung CY, Sakurai H, Chen KH, Ho HY. 2017. Anti-enterovirus 71 activities of Melissa officinalis extract and its biologically active constituent rosmarinic acid. Sci Rep 7:12264. https://doi.org/10.1038/s41598-017-12388-2.
56. Ho HY, Cheng ML, Weng SF, Leu YL, Chiu DT. 2009. Antiviral effect of epigallocatechin gallate on enterovirus 71. J Agric Food Chem 57:6140–6147. https://doi.org/10.1021/jf901128u.
57. Chen SG, Cheng ML, Chen KH, Horng JT, Liu CC, Wang SM, Sakurai H, Leu YL, Wang SD, Ho HY. 2017. Antiviral activities of Schizonepeta tenuifolia Briq. against enterovirus 71 in vitro and in vivo. Sci Rep 7:935. https://doi.org/10.1038/s41598-017-01110-x.
58. Liang CT, Chueh LL, Pang VF, Zhuo YX, Liang SC, Yu CK, Chiang H, Lee CC, Liu CH. 2007. A non-biotin polymerized horseradish-peroxidase method for the immunohistochemical diagnosis of canine distemper. J Comp Pathol 136:57–64. https://doi.org/10.1016/j.jcpa.2006.11.002.
59. Lee JK, Tansey MG. 2013. Microglia isolation from adult mouse brain. Methods Mol Biol 1041:17–23. https://doi.org/10.1007/978-1-62703-520-0_3.
60. Dionne KR, Tyler KL. 2013. Slice culture modeling of central nervous system (CNS) viral infection. Methods Mol Biol 1078:97–117. https://doi.org/10.1007/978-1-62703-640-5_9.
61. Spandidos A, Wang X, Wang H, Seed B. 2010. PrimerBank: a resource of human and mouse PCR primer pairs for gene expression detection and quantification. Nucleic Acids Res 38:D792–D799. https://doi.org/10.1093/nar/gkp1005.
62. Vinet J, Weering HR, Heinrich A, Kalin RE, Wegner A, Brouwer N, Heppner FL, Rooijen N, Boddeke HW, Biber K. 2012. Neuroprotective function for ramified microglia in hippocampal excitotoxicity. J Neuroinflammation 9:27. https://doi.org/10.1186/1742-2094-9-27.
63. Council of Agriculture (Taiwan). 2018. Guide for the care and use of laboratory animals. Council of Agriculture, Executive Yuan, Taipei, Taiwan.